This article has been accepted for publication in a future issue of this journal, but has not been fully edited. Content may change prior to final publication. Citation information: DOI 10.1109/JIOT.2018.2875428, IEEE Internet of Things Journal

RSSI-based Heading Control for Robust Long-Range Aerial Communication in UAV Networks

Jing Yan, *Member, IEEE*, Haiyan Zhao, Xiaoyuan Luo, Cailian Chen, *Member, IEEE*, and Xinping Guan, *Fellow, IEEE*

***Abstract*—Directional antenna-based aerial networking(DAAN) is referred as a promising technology to meet the dynamic data demands for unmanned aerial vehicles (UAVs). However, the narrow radiation pattern of directional antennas and the mobility of UAVs make it challenging to form a robust DAAN. This paper presents a heading control strategy for UAV-carried directional antennas to establish a robust long-range aerial communication channel. The heading control process is mainly divided into two phases, i.e., position estimation and angle adjustment. In the first phase, a proportional-derivative based tracking controller is designed for each UAV to ensure the consistency of heights, pitch and roll angles. Particularly, the received signal strength indicator (RSSI) is adopted as an auxiliary measuring component, and then a consensus-based unscented Kalman filtering (UKF) algorithm is developed to estimate the position of UAVs. With the estimated position information, a feedback-based heading controller is designed for directional antenna in the second phase to enable robust long-range aerial communication channel. Moreover, the convergence conditions and Cramér-Rao lower bounds are also provided. Finally, simulation results are presented to demonstrate the effectiveness of the proposed strategy. It is shown that the influence of malicious measurements can be reduced, and the signal strength can be significantly improved as compared with the omni-directional antenna based works.**

***Keywords*—Unmanned aerial vehicles (UAVs), aerial networking, received signal strength indicator (RSSI), directional antennas.**

I. Introduction

UNMANNED aerial vehicles (UAVs) have attracted increasing interest in the past decade for various applications, such as disaster rescue, photography, cargo delivery and inspection (e.g., see [1]–[3] and references therein). For the application of UAVs, one of the most promising technologies is to provide *on-demand* emergency communication. In emergency scenarios, the fixed communication infrastructures (e.g., Wi-Fi and cellular signals) are destroyed or do not exist. As a result, it is urgent to quickly deploy UAV-carried communication infrastructure to support urgent or ad hoc communication. This is especially appealing for the applications of internet of things (IoT), where UAVs can be regarded as terminal devices connected in the ubiquitous network. Compared with existing technologies such as satellite communication, UAV-carried communication brings several advantages, including on-demand and rapid deployment, high-rate data transmission, and strong self-organization capability.

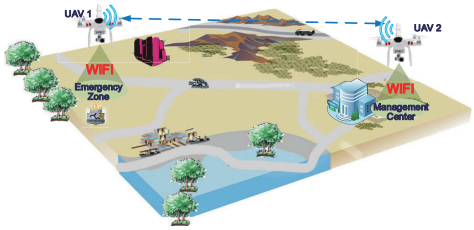

Fig. 1: Communication structure of a typical DAAN system, where a directional antenna is mounted on each UAV to provide air-to-air communication links between UAVs. In addition, an omnidirectional Wi-Fi router is enquired on each UAV to provide ground-to-air and air-to-ground communication links between UAV and terminals.

Generally speaking, the studies on UAV-carried communication can be classified into four categories, i.e., ubiquitous coverage [4]–[6], data relaying [7]–[10], data collection [11], [12], and secure communication [13], [14]. In these studies, *omni-directional* antennas are widely used to support communication services, due to their simplicity in networking design and implementation. However, the network throughput using omni-directional antennas is restricted by the limited communication range of UAVs. For instance, a typical Wi-Fi device can only extend its signal up to 100 meters [15]. Although the communication range can be extended with added transmission power, the extension is at a cost of additional battery payload for UAVs, which will significantly reduce the flight time of UAVs. Fortunately, the *directional* antennas provide us an appealing solution to extend the communication range. Of note, the directional antennas concentrate their transmitting or receiving capabilities to a certain direction. Compared with omni-directional antennas, the transmission with directional antennas can obtain a higher degree of the spatial reuse mechanism, whose transmission range is usually larger than that of omni-directional antenna. Due to these advantages, we are more interested in designing a directional antenna-based aerial networking (DAAN) system. The communication structure for a typical DAAN system is shown in Figure 1.

To establish a robust long-range DAAN system, the following critical challenges have to be addressed.

This work was partially supported by NSFC under 61873345 and 61873228, by Youth Talent Support Program of Hebei Province under BJ2018050, by Teturned Overseas Chinese Scholar Foundation for Hebei Province under C201829, and by Civil-military Integration Foundation of Hebei under 2018B.

J. Yan, H. Zhao and X. Luo are with the Institute of Electrical Engineering, Yanshan University, Qinhuangdao, 066004, China (e-mail: jyan@ysu.edu.cn, hyzhao@stumail.ysu.edu.cn, xyluo@ysu.edu.cn)

C. Chen and X. Guan are with the Department of Automation, Shanghai Jiao Tong University, Shanghai, 200240, China (email: xpguan@sjtu.edu.cn)

This article has been accepted for publication in a future issue of this journal, but has not been fully edited. Content may change prior to final publication. Citation information: DOI 10.1109/JIOT.2018.2875428, IEEE Internet of Things Journal

- *Narrow radiation patterns of directional antennas.* Different from omni-directional antennas, the directional antennas have narrow radiation patterns. As a consequence, DAAN requires directional antennas to be well aligned despite environmental disturbances. The performance of aerial communication channel can significantly degrade if directional antennas are not well aligned.
- *Mobility of UAVs.* It is noted that terrestrial networks are usually static. However, UAVs in DAAN often have active mobility derived by powerplant, or passive mobility caused by winds. Due to the mobility of UAVs, the heading angles of directional antennas are time-varying. Therefore, the mobility of UAVs should be considered to guarantee the effectiveness of heading control.

To address the above challenges, we study the issue of received signal strength indicator (RSSI) based heading control for robust long-range aerial communication in DAAN system. We first construct an integrated state and measurement model for directional antennas and UAVs. Then, a proportional-derivative (PD) based tracking controller is developed for each UAV to ensure the consistency of heights, pitch and roll angles. Based on this, a consensus-based unscented Kalman filtering (UKF) algorithm is developed to estimate the position of UAVs. With the estimated position information, the heading controller for directional antennas can be designed to robust long-range aerial communication channel. Main contributions of this paper lie in the following two aspects.

1) *An integrated state and measurement model for the co-design of communication and control strategies.* The integrated model consists of UAV dynamics, directional antenna dynamics, GPS measurements and RSSI measurements. It is noted that this model integrates the UAV dynamics into the heading control of directional antennas, which allows the co-design of communication and control strategies. Different from the existing works [16], [17], the UAV dynamics in this paper have nonlinear property with six freedoms, while the initial heights of UAVs are not required to be equal.
2) *Consensus-based heading control for directional antennas to bias the weights of each estimator in GPS/RSSI Fusion.* We develop a consensus-based UKF algorithm to estimate the position of UAVs, whose convergence conditions and Cramér-Rao lower bounds are also given. Meanwhile, a feedback-based heading controller is designed for directional antennas to enable stable air-to-air communication channel. Through consensus fusion, the influence of malicious measurements can be reduced, and signal strength can be improved as compared with omni-directional antenna based works.

II. Related Works

For the heading control of directional antennas, a global positioning system (GPS) based tracking approach was designed in [18] to improve the data transmission performance. In [19], a blind beam-based tracking method was proposed for Ka-band UAV-satellite communication system. In [20], the heading control of directional antenna was formulated as the non-deterministic polynomial (NP) hard problem, and then a bottom-up based algorithm was introduced to solve it. Also of relevance, references [21], [22] provided two heading control mechanisms to achieve robust long-range communication links for directional antennas. In these studies, GPS is required for the heading control of directional antennas. However, in some emergency (e.g., earthquake and tsunami) or indoor situations, the GPS signals are usually unstable or lacked, because the line-of-sight transmission between receivers (i.e., UAVs) and satellites is not possible. The absence of GPS limits the applications of these approaches in DAAN system.

On the aspect of heading control in GPS-denied environment, some algorithms have been developed to estimate the positions of UAVs, with additional deployment of on-board sensors such as camera and laser [24], [25]. In particular, a UAV-carried vision-based monitoring system was presented in [26], while the heuristic optimization technique was applied in [27] to determine the optimal orientations. However, camera-based approaches require sufficient lightings for the clear recognition of UAVs, and laser-based approaches are easily affected by the environment disturbances. It is noted that, RSSI uses the path loss to measure the relative position between transmitting and receiving antennas, wherein additional sensing components are not required for UAVs. Inspired by this, some researchers adopt the RSSI to estimate the position information. For instance, a RSSI-based UAV tracking control strategy was developed in [28]. Of interest, an active antenna tracking system was designed in [29] to enhance the communication capabilities of mobile robot. However, the major focus in the above studies is the design of communication protocol to keep antenna alignment, and very few works have considered both the antenna alignment and UAV mobility. As we know, the heading control of directional antennas is highly constrained by the mobility of UAVs. References [16], [17] developed and implemented a solution for the RSSI-based heading control of directional antennas in DAAN system, wherein the antenna alignment and UAV mobility are both considered. Nevertheless, the UAV dynamics in [16], [17] were simplified as second-order *linear* differential equations. As it was pointed in [30], the UAV dynamics have *nonlinear* property with six freedoms. With consideration of nonlinear UAV dynamics, how to design a RSSI-based heading controller for directional antennas is largely unexplored.

It should be stressed that, most of the existing research relies on single measurement, e.g., GPS or RSSI. As it was pointed in [31], the fusion of all available measurements can yield improved estimator accuracy and robustness. Inspired by this, the heading control of directional antennas needs to be pursued through fusing data generated from existing measurements in DAAN system. Thereby, we attempt to bias the weights of GPS and RSSI measurements in the fusion process in accordance with signal stability. It is noted that the *consensus* involves a set of local rules to regulate the updating iteration, and then an agreement regarding a certain quantity of interest is reached [32], [33]. In the ground breaking work [34], Olfati-Saber adopted the consensus-based Kalman algorithm to improve the tracking accuracy of multi-agent systems. Several other consensus-based algorithms were developed in [35]–[37] and

This article has been accepted for publication in a future issue of this journal, but has not been fully edited. Content may change prior to final publication. Citation information: DOI 10.1109/JIOT.2018.2875428, IEEE Internet of Things Journal

TABLE I: Main notations used in this paper.

x_i	State of UAV i along X coordinate
y_i	State of UAV i along Y coordinate
z_i	State of UAV i along Z coordinate
φ_i	Angle of UAV i along pitch
ψ_i	Angle of UAV i along roll
ϕ_i	Angle of UAV i along yaw
$v_{i,x}$	Velocity of UAV i along X coordinate
$v_{i,y}$	Velocity of UAV i along Y coordinate
$v_{i,z}$	Velocity of UAV i along Z coordinate
$\vec{p}_i$	Angle velocity of UAV i along pitch
$\vec{q}_i$	Angle velocity of UAV i along roll
$\vec{r}_i$	Angle velocity of UAV i along yaw
δ	Sampling period
g	Gravity acceleration
l	Half length of each UAV
m	Mass of each UAV
$\mathcal{C}$	Force to moment scaling factor

references therein. Nevertheless, due to the narrow radiation pattern of directional antennas and the mobility of UAVs, these approaches cannot be directly applied to the DAAN system. How to provide a consensus-based solution that involves GPS and RSSI measurements to provide robust long-range aerial communication channel is largely unexplored.

III. Modeling and Problem Formulation

Considering the DAAN system as shown in Figure 1, we would like to establish a robust long-range aerial communication channel. To achieve this goal, the heading angles of directional antennas on the two UAVs need to be well aligned with each other. However, the narrow radiation pattern of directional antennas and the mobility of UAVs make it difficult to achieve this task. For this reason, we first develop an integrated state and measurement model for the co-design of communication and control strategies. Then, we summarize the problems waiting to be solved. Table I shows the main notations used in this paper for $i \in \{1, 2\}$.

A. Integrated State Model for UAVs and Directional Antennas

In DAAN system, each UAV is installed with a directional antennas, and the mobility of UAVs plays an important role in the heading control of directional antennas. In view of this, we adopt nonlinear Lagrange equations to formulate the UAV dynamics. Particularly, body-fixed reference frame(BRF) and inertial reference frame(IRF) are used to describe the UAV dynamics, as shown in Figure 2. Accordingly, the dynamics of UAV i are given as [30]

$$\begin{aligned}
v_{i,x}(k+1) &= v_{i,x}(k) + [u_{i,1}(k)A_i(k) - \tfrac{K_1}{m}v_{i,x}(k)]\delta,\\
v_{i,y}(k+1) &= v_{i,y}(k) + [u_{i,1}(k)\vec{B}_i(k) - \tfrac{K_2}{m}v_{i,y}(k)]\delta,\\
v_{i,z}(k+1) &= v_{i,z}(k) + [\tfrac{\tau_i(k)}{m}C_i(k) - g - \tfrac{K_3}{m}v_{i,z}(k)]\delta,\\
\vec{p}_i(k+1) &= \vec{p}_i(k) + [u_{i,2}(k) - \tfrac{lK_4}{I_1}\vec{p}_i(k)]\delta,
\end{aligned}$$

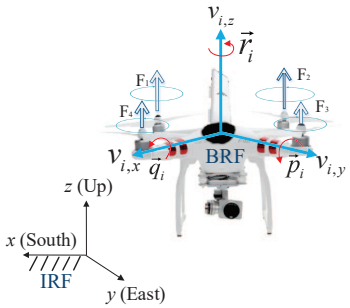

Fig. 2: The UAV i dynamics in BRF and IRF.

$$\begin{aligned}
\vec{q}_i(k+1) &= \vec{q}_i(k) + [u_{i,3}(k) - \tfrac{lK_5}{I_2}\vec{q}_i(k)]\delta,\\
\vec{r}_i(k+1) &= \vec{r}_i(k) + [u_{i,4}(k) - \tfrac{K_6}{I_3}\vec{r}_i(k)]\delta,
\end{aligned} \tag{1}$$

where $A_i = \cos(\phi_i)\sin(\varphi_i)\cos(\psi_i) + \sin(\phi_i)\sin(\psi_i)$, $\vec{B}_i = \cos(\phi_i)\sin(\varphi_i)\cos(\psi_i) - \cos(\phi_i)\sin(\psi_i)$, and $C_i = \cos(\phi_i)\cos(\psi_i)$. In addition, $u_{i,1} = (F_1+F_2+F_3+F_4)/m$ and $u_{i,4} = \mathcal{C}(F_1-F_2+F_3-F_4)/I_3$ are the virtual control inputs along X coordinate and yaw, respectively. τ_i, $u_{i,2}$ and $u_{i,3}$ denote the exerted forces along Z coordinate, pitch and roll, respectively. I_1, I_2 and I_3 are the inertia moments. $K_1, ..., K_6$ are the drag coefficients. Moreover, F_1, F_2, F_3 and F_4 represent the thrusts which are generated by four rotors.

With respect to (1), the state of UAV i is defined as $(x_i(k), y_i(k), z_i(k), \varphi_i(k), \psi_i(k), \phi_i(k))$. In view of the relationship between velocity and state, the state model is described as

$$\begin{bmatrix} x_i(k+1)\\ y_i(k+1)\\ z_i(k+1)\\ \varphi_i(k+1)\\ \psi_i(k+1)\\ \phi_i(k+1) \end{bmatrix} = \begin{bmatrix} x_i(k)\\ y_i(k)\\ z_i(k)\\ \varphi_i(k)\\ \psi_i(k)\\ \phi_i(k) \end{bmatrix} + \begin{bmatrix} v_{i,x}(k)\delta\\ v_{i,y}(k)\delta\\ v_{i,z}(k)\delta\\ \vec{p}_i(k)\delta\\ \vec{q}_i(k)\delta\\ \vec{r}_i(k)\delta \end{bmatrix}. \tag{2}$$

Remark 1: It is noted that the UAV dynamics in [16], [17] are described as second-order linear differential equations. In practice, the UAV dynamics have nonlinear property. Therefore, we use (1) and (2) to describe the nonlinear dynamics of UAVs, through which the UAV mobility can be accurately incorporated into the heading control of directional antennas.

Without loss of generality, it is assumed that the yaw angle of directional antenna can autonomously adjust, while the angles along pitch and roll are fixed on UAV. Then, the movement of directional antenna can be divided into the following two aspects: 1) active movement that is driven by rotating motors; 2) passive movement that is driven by the mobility of UAV. Accordingly, the dynamics of directional antenna i for the active movement are given as

$$\begin{aligned}
\theta_i^*(k+1) &= \theta_i^*(k) + \omega_i(k)\delta\\
J\omega_i(k+1) &= J\omega_i(k) + \tau_i^*(k)\delta,
\end{aligned} \tag{3}$$

where $i \in \{1, 2\}$, θ_i^* is the angle associated with the active movement of antenna i relative to the UAV frame, J is the moment of inertia for the antenna body, ω_i represents the angle velocity of antenna i due to its heading control, and τ_i^* denotes

This article has been accepted for publication in a future issue of this journal, but has not been fully edited. Content may change prior to final publication. Citation information: DOI 10.1109/JIOT.2018.2875428, IEEE Internet of Things Journal

the control torque to steer the antenna to a desired angle.

Based on (1) and (3), the state model for directional antenna i can be updated as

$$\theta_i(k+1) = \theta_i(k) + (\omega_i(k) + \vec{r}_i(k))\delta, \tag{4}$$

where θ_i is the heading angle of antenna i.

With (2) and (4), the integrated state model for UAVs and directional antennas is given as

$$X(k+1) = X(k) + B(k)U(k) + V(k), \tag{5}$$

where $X(k) = [X_1^T(k), X_2^T(k)]^T$, $B(k) = [B_1(k), 0_{7\times7}; 0_{7\times7}, B_2(k)]$, $U(k) = [U_1^T(k), U_2^T(k)]^T$ and $X_i(k+1) = X_i(k) + B_i(k)U_i(k)$. For $i \in \{1,2\}$, $X_i(k) = [x_i(k), y_i(k), z_i(k), \varphi_i(k), \psi_i(k), \phi_i(k), \theta_i(k)]^T$ and $U_i(k) = [v_{i,x}(k), v_{i,y}(k), v_{i,z}(k), \vec{p}_i(k), \vec{q}_i(k), \vec{r}_i(k), \omega_i(k)]^T$ denote the state and local input for UAV i, respectively. In addition, $B_i(k) = [\delta_1, 0_{5\times2}; 0_{2\times5}, \delta_2]$, where δ_1 =diag$(\delta, \delta, \delta, \delta, \delta)$ and $\delta_2 = [\delta, 0; \delta, \delta]$. $V(k) = [V_1^T(k), V_2^T(k)]^T$ is the additive process noise of zero mean with covariance matrix $Q(k)$.

B. Measurement Model for UAVs and Directional Antennas

1. Self-position measurement: GPS unit is mounted on each UAV. As a result, UAV i utilizes GPS to measure its own position $[x_i, y_i, z_i]^T$, and the measurement model is

$$z_{G,i}(k) = H_{G,i}(k)X(k) + \varpi_{G,i}(k), \tag{6}$$

where $H_{G,i} = [1, 0, 0, 0, 0, 0, 0, 0, 0, 0, 0, 0, 0, 0; 0, 1, 0, 0, 0, 0, 0, 0, 0, 0, 0, 0, 0, 0; 0, 0, 1, 0, 0, 0, 0, 0, 0, 0, 0, 0, 0, 0]$ denotes the self-position measurement matrix, $\varpi_{G,i} \in \mathcal{R}^3$ represents the white Gaussian noise of zero mean with covariance matrix $R_{G,i}(k)$, and $i \in \{1,2\}$.

2. GPS-based measurement of the remote UAV: To acquire the desired heading angle of directional antenna, the remote UAV j transmits its position $[x_j, y_j, z_j]^T$ to UAV i through the low data-rate wireless communication module, where $j \in \{1,2\}/\{i\}$. Correspondingly, the measurement model is

$$z_{G,i}^{\#}(k) = H_{G,i}^{\#}(k)X(k) + \varpi_{G,i}^{\#}(k), \tag{7}$$

where $H_{G,i}^{\#} = [0, 0, 0, 0, 0, 0, 0, 1, 0, 0, 0, 0, 0, 0; 0, 0, 0, 0, 0, 0, 0, 0, 0, 1, 0, 0, 0, 0; 0, 0, 0, 0, 0, 0, 0, 0, 0, 0, 1, 0, 0, 0]$ is the measurement matrix for UAV j, and $\varpi_{G,i}^{\#} \in \mathcal{R}^3$ denotes the white Gaussian noise of zero mean with covariance matrix $R_{G,i}^{\#}(k)$.

3. RSSI-based measurement of the remote UAV: It is noted that RSSI uses the path loss to measure the relative position between transmitting and receiving antennas. Then, we adopt RSSI to estimate the position of remote UAV in GPS-denied environment, and the directional antanna of Nanostation LocoM5 [38] is selected for the RSSI measurement. With respect to this, the experimental data is shown in Figure 3, where the direction of receiving antenna is fixed in each 10min while the direction of transmitting antenna turn 360°. It is clear that the signal strength is the strongest when two directional antennas point toward each other, and the signal strength is reduced when the two directional antennas deviate each other.

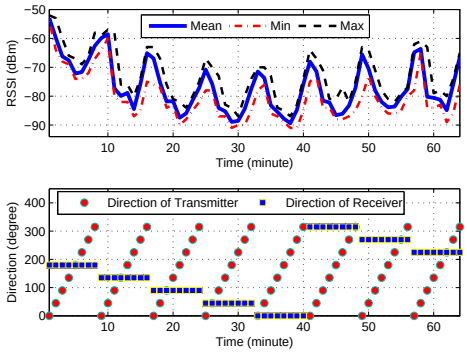

Fig. 3: Experimental data for RSSI measurements [16].

Then, the measured RSSI at receiving antenna i is given as

$$\begin{aligned} z_{R,i}(k) &= K_i + K_{t,j}\cos^2\tfrac{\gamma_j(k)-\theta_j(k)}{2} - L_f\,|_{\text{dBm}} \\ &\quad + K_{r,i}\cos^2\tfrac{\gamma_i(k)-\theta_i(k)}{2} + \varpi_{R,i}(k), \end{aligned} \tag{8}$$

where $i \neq j$, $i,j \in \{1,2\}$. γ_i and γ_j are the desired heading angles for directional antennas i and j, respectively. $K_i = P_{t,j}\,|_{\text{dBm}} + G_{t,j}^{\min}\,|_{\text{dBm}} + G_{r,i}^{\min}\,|_{\text{dBm}}$, $K_{t,j} = G_{t,j}^{\max}\,|_{\text{dBm}} - G_{t,j}^{\min}\,|_{\text{dBm}}$ and $K_{r,i} = G_{r,i}^{\max}\,|_{\text{dBm}} - G_{r,i}^{\min}\,|_{\text{dBm}}$. $P_{t,j}\,|_{\text{dBm}}$ represents the output power of transmitting antenna j. $G_{t,j}^{\max}\,|_{\text{dBm}}$ and $G_{t,j}^{\min}\,|_{\text{dBm}}$ are the maximum and minimum gains of transmitting antenna j, respectively. $L_f\,|_{\text{dBm}} = 20\lg(4\pi d/\lambda)$ is the free-space loss, where λ is the wavelength and d is the distance between receiving and transmitting antennaes. $G_{r,i}^{\max}\,|_{\text{dBm}}$ and $G_{r,i}^{\min}\,|_{\text{dBm}}$ are the maximum and minimum gains of receiving antenna i, respectively. It is assumed that $P_{r,i}\,|_{\text{dBm}}$, $G_{t,j}^{\max}\,|_{\text{dBm}}$, $G_{t,j}^{\min}\,|_{\text{dBm}}$, $G_{r,i}^{\max}\,|_{\text{dBm}}$ and $G_{r,i}^{\min}\,|_{\text{dBm}}$ are the constants which can be obtained from either antenna datasheet or experimental studies. In addition, $\varpi_{R,i} \in \mathcal{R}$ is the white Gaussian noise of zero mean with covariance $R_{R,i}(k)$. In our previous work [16], we have given a detailed construction process for the RSSI measurement model. Due to page limitation, please see [16] for the detailed results.

Remark 2: Although the RSSI measurement (8) is derived from free-space path loss model [39], there are still some differences. For instance, the transmitter and receiver gains in (8) are time-varying, while the gains in [39] are fixed. The reason associated with design is the narrow radiation patterns of directional antennas, i.e., the directional pattern.

C. Problem Formulation

Problem: Consider the scenario of DAAN system as shown in Figure 1. Three problems are required to be solved.

1) At time step $k = 0$, UAV j uses altimetric sensor to measure its height z_j, and then transmits it to UAV i. Based on this, a tracking controller is sought for UAV i to ensure the consistency of heights, pitch and roll angles. This problem is reduced to guarantee $\varphi_i \to 0$, $\psi_i \to 0$ and $z_i \to z_j$ with a limited time interval.

This article has been accepted for publication in a future issue of this journal, but has not been fully edited. Content may change prior to final publication. Citation information: DOI 10.1109/JIOT.2018.2875428, IEEE Internet of Things Journal

2) With the same heights, pitch and roll angles, we attempt to design a consensus-based algorithm that involves GPS and RSSI measurements to provide robust long-range aerial communication. This problem is reduced to the estimation of $[x_j, y_j, z_j]^T$ with the fusion of GPS and RSSI measurements according to (7) and (8).
3) With the estimated UAV positions, the desired heading angle γ_i can be obtained. Then, a feedback-based heading controller is sought for directional antenna i to track its desired heading angle γ_i, i.e., $\theta_i \to \gamma_i$ with limited time interval, such that the signal strength between transmitting and receiving UAVs can be enhanced.

IV. Consensus-based Heading Control

In this section, we first design a PD-based tracking controller for UAV i to ensure the consistency of heights, pitch and roll angles. Then, the position estimations of UAV i and remote UAV j are presented, respectively. Finally, a feedback-based heading controller is developed for directional antennas.

A. PD-based Tracking Controller

As discussed above, the initial heights of UAV i and remote UAV j are not required to be equal. Then, we give two possible solutions to align the transmitting and receiving antennas, as shown in Figure 4. For Solution 1, the heights of two UAVs are fixed, while the pitch, roll and yaw angles are adjusted to align the directional antennas. Due to the difference of heights, the pitch and roll angles (i.e., φ_i and ψ_i for $i \in \{1, 2\}$) in Solution 1 are not always be zeros. Clearly, this design can lead to the gravity unbalance of UAVs. Alternatively, the heights of UAVs in Solution 2 can be adjusted, while the desired pitch and roll angles are set to be zeros. It is obvious that Solution 2 can avoid the occurrence of gravity imbalance. Inspired by this, we adopt Solution 2 to design a [illegible]-based tracking controller for each UAV, whose aim is to guarantee $\varphi_i(k) \to 0$, $\psi_i(k) \to 0$ and $z_1(k) \to z_2(k)$ [illegible]

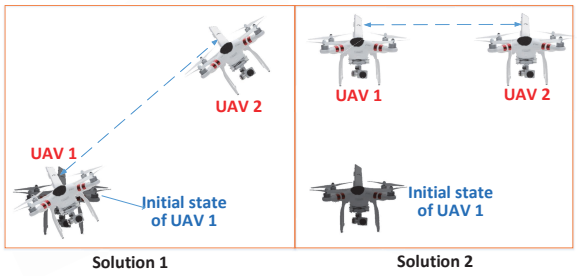

Fig. 4: Solutions to align the directional antennas.

Then, the PD-based tracking controller for height of UAV i is developed as

$$\tau_i(k) = \frac{k_{i,z1}e_{i,z}(k) + k_{i,z2}e^{\triangle}_{i,z}(k) + mg}{\cos(\phi_i(k))\cos(\psi_i(k))}, \quad (9)$$

where $i \neq j$, $i, j \in \{1, 2\}$. $k_{i,z1} \in \mathcal{R}^+$ and $k_{i,z2} \in \mathcal{R}^+$ are the proportional and derivative gains, respectively. It is defined that $e_{i,z}(k) = z_j(k) - z_i(k)$ and $e^{\triangle}_{i,z}(k) = v_{j,z}(k) - v_{i,z}(k)$. In particular, $\phi_i(k) \in (-\pi/2, \pi/2)$ and $\psi_i(k) \in (-\pi/2, \pi/2)$.

Similarly, the PD-based tracking controllers for the pitch and roll angles of UAV i are designed as

$$u_{i,2}(k) = k_{i,\varphi 1}e_{i,\varphi}(k) + k_{i,\varphi 2}e^{\triangle}_{i,\varphi}(k), \quad (10)$$
$$u_{i,3}(k) = k_{i,\psi 1}e_{i,\psi}(k) + k_{i,\psi 2}e^{\triangle}_{i,\psi}(k), \quad (11)$$

where $k_{i,\varphi 1} \in \mathcal{R}^+$ and $k_{i,\psi 1} \in \mathcal{R}^+$ are the proportional gains. $k_{i,\varphi 2} \in \mathcal{R}^+$ and $k_{i,\psi 2} \in \mathcal{R}^+$ are the derivative gains. Meanwhile, it is defined that $e_{i,\varphi}(k) = -\varphi_i(k)$, $e^{\triangle}_{i,\varphi}(k) = -\vec{p}_i(k)$, $e_{i,\psi}(k) = -\psi_i(k)$ and $e^{\triangle}_{i,\psi}(k) = -\vec{q}_i(k)$. Referring to [40], the PD-based tracking controllers, i.e., (9), (10) and (11), can guarantee the convergence of system (1).

B. Self-position Estimation for UAV i

When local GPS signals are available, UKF algorithm is used to estimate the self-position of UAV i. Due to the nonlinear dynamics of the measurement model, conventional Kalman Filtering is not applicable. Extended Kalman Filtering (EKF) has been developed to address the nonlinearity [41]. However, it requires computing the Jacobian matrices and hence imposes difficulty for effective implementation. UKF, instead, provides an effective way for the state estimation of nonlinear systems by using sampling techniques [42], [43]. Here, the estimator of $X(k)$ is denoted as $\hat{X}(k)$, and the error covariance matrix of $\hat{X}(k)$ is denoted as $P(k)$. It is noted that the self-position estimation for UAV i does not require the update of full state $X(k)$, wherein only a part of $X(k)$, i.e., $[x_1(k), y_1(k), z_1(k), \phi_1(k), x_2(k), y_2(k), z_2(k), \phi_2(k)]$ is needed. We here show the full state dynamics for the convenience of reusing UKF in Section IV-C.

Step 1: Initialization. At $k = 1$, the computation algorithm begins with the following initial conditions

$$\hat{X}(0) = E[X(0)]$$
$$P(0) = E[(X(0) - \hat{X}(0))(X(0) - \hat{X}(0))^T]. \quad (12)$$

Step 2: Selection of sigma points. At the start of time step k, a set of $2L+1$ sigma points are chosen based on the estimated state $\hat{X}(k-1)$ and the error covariance matrix $P(k-1)$, i.e.,

$$\mathcal{X}_s(k-1) = [\hat{X}(k-1), \hat{X}(k-1) \pm (\zeta\sqrt{P(k-1)})_m], \quad (13)$$

where $\mathcal{X}_s$ is the sth column of $\mathcal{X}$ and $s = 0, \ldots, 2L$. $\zeta = \sqrt{L + \varsigma}$, where ς is a composite scaling parameter, and $L = 14$. $(\cdot)_m$ denotes the mth column of a matrix.

Step 3: Iteration update. Introducing sigma points into the state, the prediction state $\mathcal{X}_s(k|k-1)$ can be expressed as

$$\mathcal{X}_s(k\,|k-1) = \mathcal{X}_s(k-1) + B(k-1)U(k-1), s = 0, \ldots, 2L \quad (14)$$

A priori state estimation is approximated by using a weighted sample mean

$$\hat{X}(k\,|k-1) = \sum_{s=0}^{2L} W_s \mathcal{X}_s(k\,|k-1) \quad (15)$$

This article has been accepted for publication in a future issue of this journal, but has not been fully edited. Content may change prior to final publication. Citation information: DOI 10.1109/JIOT.2018.2875428, IEEE Internet of Things Journal

and the covariance matrix is calculated as

$$\begin{aligned} & P(k\,|k-1\,) \\ = \;& \textstyle\sum_{s=0}^{2L} W_s[\mathcal{X}_s(k\,|k-1\,) - \hat{X}(k\,|k-1\,)] \\ & \times[\mathcal{X}_s(k\,|k-1\,) - \hat{X}(k\,|k-1\,)]^T + Q(k) \end{aligned} \tag{16}$$

where $W_s{=}\varsigma/(L{+}\varsigma)$ if $s{=}0$, otherwise, $W_s{=}1/(2(L{+}\varsigma))$.

Update the priori state estimation with the following rule

$$\begin{aligned} & \mathcal{X}_s(k\,|k-1\,) \\ = \;& [\hat{X}(k\,|k-1\,), \hat{X}(k\,|k-1\,)\pm(\gamma\sqrt{P(k\,|k-1\,)})_m]. \end{aligned} \tag{17}$$

Step 4: Measurement update. Mapping $\mathcal{X}_s(k\,|k-1\,)$ into measurement Equation (6), the unscented transform of the self-position observations is computed as

$$\mathcal{Z}_{G,i,s}(k\,|k-1\,) = H_{G,i}(k\,|k-1\,)\mathcal{X}_s(k\,|k-1\,) \tag{18}$$

The priori measurement estimation is approximated by using the weighted mean value

$$\hat{z}_{G,i}(k\,|k-1\,) = \textstyle\sum_{s=0}^{2L} W_s \mathcal{Z}_{G,i,s}(k\,|k-1\,) \tag{19}$$

For UAV i, the self-position measurement covariance matrix $P_{i,\hat{z}_{G,i}(k)\hat{z}_{G,i}(k)}$ and self-position measurement cross-covariance matrix $P_{i,\hat{X}(k)\hat{z}_{G,i}(k)}$ are updated as

$$\begin{aligned} & P_{i,\hat{z}_{G,i}(k)\hat{z}_{G,i}(k)} \\ = \;& \textstyle\sum_{s=0}^{2L} W_s[\mathcal{Z}_{G,i,s}(k\,|k-1\,){-}\hat{z}_{G,i}(k\,|k-1\,)] \\ & \times[\mathcal{Z}_{G,i,s}(k\,|k-1\,){-}\hat{z}_{G,i}(k\,|k-1\,)]^T{+}R_{G,i}(k) \end{aligned} \tag{20}$$

$$\begin{aligned} & P_{i,\hat{X}(k)\hat{z}_{G,i}(k)} \\ = \;& \textstyle\sum_{s=0}^{2L} W_s[\mathcal{X}_s(k\,|k-1\,) - \hat{X}(k\,|k-1\,)] \\ & \times[\mathcal{Z}_{G,i,s}(k\,|k-1\,) - \hat{z}_{G,i}(k\,|k-1\,)]^T. \end{aligned} \tag{21}$$

Step 5: Kalman Filtering Update. Finally, we can update the Kalman gain $\mathcal{K}_i(k)$, the estimated state $\hat{X}(k)$, and variance matrix $P(k)$ through the following update rules

$$\begin{aligned} \mathcal{K}_i(k) &= P_{i,\hat{X}(k)\hat{z}_{G,i}(k)} P^{-1}_{i,\hat{z}_{G,i}(k)\hat{z}_{G,i}(k)} \\ \hat{X}(k) &= \hat{X}(k\,|k-1\,) + \mathcal{K}_i(k)(z_{G,i}(k) - \hat{z}_{G,i}(k\,|k-1\,)) \\ P(k) &= P(k\,|k-1\,) - \mathcal{K}_i(k) P_{i,\hat{z}_{G,i}(k)\hat{z}_{G,i}(k)} \mathcal{K}_i^T(k). \end{aligned} \tag{22}$$

C. Estimation of Remote UAV j's Position

In this section, we develop a consensus-based UKF algorithm that involves GPS and RSSI measurements to estimate the position of remote UAV j. Of note, it is assumed that at least one of GPS or RSSI signal is feasible. Under this assumption, GPS of UAV j can successfully transmit to UAV i through low-rate omni-directional communication module, or RSSI is feasible to UAV i. If only the GPS signal is available, Steps 1 and 2 are similar to (12) and (13) and hence are omitted. The main difference is the observation process in Step 4. In particular, the unscented transform of GPS observations is replaced with $\mathcal{Z}^{\#}_{G,i,s}(k\,|k-1\,)$ and $\hat{z}^{\#}_{G,i}(k\,|k-1\,)$ with definitions similar to (18) and (19), respectively.

Accordingly, the rest of estimation steps can be provided. For instance, the Kalman gain is given as

$$\mathcal{K}_{G,i}(k) = P_{i,\hat{X}(k)\hat{z}^{\#}_{G,i}(k)} P^{-1}_{i,\hat{z}^{\#}_{G,i}(k)\hat{z}^{\#}_{G,i}(k)}. \tag{23}$$

Then, the state estimator $\hat{X}_G(k)$ and variance matrix $P_G(k)$ are given through the following update rules

$$\begin{aligned} \hat{X}_G(k) &= \hat{X}(k\,|k-1\,) + \mathcal{K}_{G,i}(k)(z^{\#}_{G,i}(k){-}\hat{z}^{\#}_{G,i}(k\,|k-1\,)) \\ P_G(k) &= P(k\,|k-1\,) - \mathcal{K}_{G,i}(k) P^T_{i,\hat{z}^{\#}_{G,i}(k)\hat{z}^{\#}_{G,i}(k)} \mathcal{K}^T_{G,i}(k) \end{aligned} \tag{24}$$

where the definitions of $P_{i,\hat{X}(k)\hat{z}^{\#}_{G,i}(k)}$ and $P_{i,\hat{z}^{\#}_{G,i}(k)\hat{z}^{\#}_{G,i}(k)}$ are similar to the ones in (20) and (21), i.e., $P_{i,\hat{z}^{\#}_{G,i}(k)\hat{z}^{\#}_{G,i}(k)} = \sum_{s=0}^{2L} W_s[\mathcal{Z}^{\#}_{G,i,s}(k\,|k-1\,) - \hat{z}^{\#}_{G,i}(k\,|k-1\,)][\mathcal{Z}^{\#}_{G,i,s}(k\,|k-1\,) - \hat{z}^{\#}_{G,i}(k\,|k-1\,)]^T + R^{\#}_{G,i}(k)$, $P_{i,\hat{X}(k)\hat{z}^{\#}_{G,i}(k)} = \sum_{s=0}^{2L} W_s [\mathcal{X}_s(k|k-1)\text{-}\hat{X}(k|k-1)][\mathcal{Z}^{\#}_{G,i,s}(k\,|k-1)\text{-}\hat{z}^{\#}_{G,i}(k|k-1)]^T$. $\kappa_{G,i}(k) = z^{\#}_{G,i}(k){-}\hat{z}^{\#}_{G,i}(k\,|k-1\,)$ is the innovation associated with this estimation, to be used in the consensus fusion.

Similarly, if only RSSI signal is valid to UAV i, RSSI can be adopted to estimate the augmented position (x_j, y_j, θ_j). Without loss of generality, it is assumed that the heights of two UAVs have reached to the same value through the tracking controller as given in Section IV-A. For clear description, the RSSI measurement in (8) is rearranged as $z_{R,i}(k) = f(X(k), W(k))$, where $W(k)$ is the measurement noise. With the initialization and selection of sigma points in (12) and (13), the measurement and priori measurement estimation of the RSSI signal can be computed as

$$\begin{aligned} \mathcal{Z}_{R,i,s}(k\,|k-1\,) &= f(X(k|k-1), W(k|k-1)) \\ \hat{z}_{R,i}(k\,|k-1\,) &= \textstyle\sum_{s=0}^{2L} W_s \mathcal{Z}_{R,i,s}(k\,|k-1\,) \end{aligned}$$

Correspondingly, the predicted measurement covariance matrix $P_{i,\hat{z}_{R,i}(k)\hat{z}_{R,i}(k)}$ and cross-covariance matrix $P_{i,\hat{X}(k)\hat{z}_{R,i}(k)}$ are updated as

$$\begin{aligned} & P_{i,\hat{z}_{R,i}(k)\hat{z}_{R,i}(k)} \\ = \;& \textstyle\sum_{s=0}^{2L} W_s[\mathcal{Z}_{R,i,s}(k\,|k-1\,) - \hat{z}_{R,i}(k\,|k-1\,)] \\ & \times[\mathcal{Z}_{R,i,s}(k\,|k-1\,) - \hat{z}_{R,i}(k\,|k-1\,)]^T + R_{R,i}(k) \\ & P_{i,\hat{X}(k)\hat{z}_{R,i}(k)} \\ = \;& \textstyle\sum_{s=0}^{2L} W_s[\mathcal{X}_s(k\,|k-1\,) - \hat{X}(k\,|k-1\,)] \\ & \times[\mathcal{Z}_{R,i,s}(k\,|k-1\,) - \hat{z}_{R,i}(k\,|k-1\,)]^T. \end{aligned}$$

Thereby, the Kalman gain $\mathcal{K}_{R,i}(k)$, the state estimator $\hat{X}_R(k)$ and variance matrix $P_R(k)$ are designed as

$$\begin{aligned} \mathcal{K}_{R,i}(k) &= P_{i,\hat{X}(k)\hat{z}_{R,i}(k)} P^{-1}_{i,\hat{z}_{R,i}(k)\hat{z}_{R,i}(k)} \\ \hat{X}_R(k) &= \hat{X}(k\,|k-1\,) + \mathcal{K}_{R,i}(k)(z_{R,i}(k) - \hat{z}_{R,i}(k\,|k-1\,)) \\ P_R(k) &= P(k\,|k-1\,) - \mathcal{K}_{R,i}(k) P_{i,\hat{z}_{R,i}(k)\hat{z}_{R,i}(k)} \mathcal{K}^T_{R,i}(k), \end{aligned} \tag{25}$$

where $\kappa_{RS,i}(k) = z_{R,i}(k) - \hat{z}_{R,i}(k\,|k-1\,)$ is the innovation associated with estimation, to be used in the consensus fusion.

In the following, we use the idea of consensus to fuse the results of $\hat{X}_G(k)$, $P_G(k)$, $\hat{X}_R(k)$ and $P_R(k)$, i.e., each UAV computes a weighted consensus of the state estimator and

This article has been accepted for publication in a future issue of this journal, but has not been fully edited. Content may change prior to final publication. Citation information: DOI 10.1109/JIOT.2018.2875428, IEEE Internet of Things Journal

variance matrix based on GPS and RSSI estimations. Thus, the refreshed results are given as

$$\hat{X}(k) = \alpha_G \hat{X}_G(k) + \alpha_R \hat{X}_R(k) \quad (26)$$
$$P(k) = \alpha_G P_G(k) + \alpha_R P_R(k), \quad (27)$$

where $\alpha_G \in \mathcal{R}^+$ and $\alpha_R \in \mathcal{R}^+$ are the weights for GPS and RSSI estimations, respectively. The weights satisfy the condition of $\alpha_G + \alpha_R = 1$. The detailed update process is summarized in Algorithm 1.

Algorithm 1: CONSENSUS based fusion algorithm

Input: Initialize $\hat{X}(0)$ and $P(0)$
Output: The state estimator $\hat{X}(k)$ and correction $P(k)$
for $k = 1 : N$ **do**
- Generate the sigma point $\mathcal{X}_s(k-1)$ using (13);
- Calculate the state $\mathcal{X}_s(k\,|k-1)$ with (14), and obtain $P(k\,|k-1)$ from (16);
- Update the state $\mathcal{X}_s(k\,|k-1)$ with (17);
- Calculate the estimates $\mathcal{Z}^{\#}_{G,i,s}(k\,|k-1)$, $\mathcal{Z}_{R,i,s}(k\,|k-1)$, $\hat{z}^{\#}_{G,i}(k\,|k-1)$ and $\hat{z}_{R,i}(k\,|k-1)$;
- Update the measurement covariance and cross-covariance matrices, i.e., $P_{i,\hat{X}(k)\hat{z}^{\#}_{G,i}(k)}$, $P_{i,\hat{z}^{\#}_{G,i}(k)\hat{z}^{\#}_{G,i}(k)}$, $P_{i,\hat{z}_{R,i}(k)\hat{z}_{R,i}(k)}$ and $P_{i,\hat{X}(k)\hat{z}_{R,i}(k)}$;
- Obtain the state estimators and corrections, i.e, $\hat{X}_G(k)$, $P_G(k)$, $\hat{X}_R(k)$ and $P_R(k)$;
- Refresh the state estimator and correction with (26) and (27).

Different from the stochastic weight in [44], the weights in this paper are deterministic. Compared with the stochastic weights, the deterministic weights in this paper can maximize the benefit of estimated state through well-adapted measurements. Meanwhile, the deterministic weights can minimize the ones that are not well-adapted, such that the influence of malicious measurements can be significantly reduced. In view of this, we define the virtual measurement for GPS signal and RSSI signal as $q_{G,i}(k) = \kappa^T_{G,i}(k) S^{-1}_{G,i}(k) \kappa_{G,i}(k)$ and $q_{RS,i}(k) = \kappa^2_{RS,i}(k) S^{-1}_{RS,i}(k)$, respectively. Particularly, it is denoted that $S_{G,i}(k) = P_{i,\hat{z}^{\#}_{G,i}(k)\hat{z}^{\#}_{G,i}(k)} + R^{\#}_{G,i}(k)$ and $S_{RS,i}(k) = P_{i,\hat{z}_{R,i}(k)\hat{z}_{R,i}(k)} + R_{R,i}(k)$. In addition, the threshold measurements of GPS and RSSI estimations are denoted as $q_{G,\max}$ and $q_{RS,\max}$, respectively. Then the deterministic weights are defined as follow. If $q_{G,i} > q_{G,\max}$ and $q_{RS,i} \leq q_{RS,\max}$, only RSSI signal is feasible, and the weights are provided as $\alpha_G = 0$ and $\alpha_R = 1$. Similarly, when $q_{G,i} \leq q_{G,\max}$ and $q_{RS,i} > q_{RS,\max}$, only GPS signal is reliable, the weights become $\alpha_G = 1$ and $\alpha_R = 0$. If $q_{G,i} \leq q_{G,\max}$ and $q_{RS,i} \leq q_{RS,\max}$, the two signals are both useful and the weights are defined as $\alpha_G = \frac{q_{G,\max} - q_{G,i}(k)}{q_{G,\max} - q_{G,i}(k) + q_{RS,\max} - q_{RS,i}(k)}$ and $\alpha_R = \frac{q_{RS,\max} - q_{RS,i}(k)}{q_{G,\max} - q_{G,i}(k) + q_{RS,\max} - q_{RS,i}(k)}$, respectively. In addition, if $q_{G,i} > q_{G,\max}$ and $q_{RS,i} > q_{RS,\max}$, the GPS signal and RSSI signal are invalid, which leads to the growth of accumulative error. Clearly, this case is out of the scope of this paper and hence is omitted.

D. Feedback-based Heading Controller Design for Antenna i

With the estimated UAV positions, the desired heading angle γ_i can be obtained for $\forall i \in \{1, 2\}$. Then, a feedback-based heading controller is sought for directional antenna i to track $\gamma_i(k)$, i.e., $\theta_i(k) \to \gamma_i(k)$ with a limited time interval. In view of (4), it is known that the heading angle $\theta_i(k)$ is a combination of $\theta^*_i(k)$ and $\Delta\phi_i(k) = \phi_i(k) - \phi_i(k-1)$, where θ^*_i is the self-movement angle and $\Delta\phi_i(k)$ is the passive-movement angle caused by the mobility of UAV. Correspondingly, the angle velocity of antenna i is a combination of $\omega_i(k)$ and $\vec{r}_i(k)$. Based on this, the desired self-movement angle of antenna i can be obtained, i.e., $\gamma^*_i(k) = \gamma_i(k) - \Delta\phi_i(k)$. As such, the heading control problem is reduced to make $\theta^*_i(k)$ converge to $\gamma^*_i(k)$ with a limited time interval.

Inspired by this, a feedback control loop is constructed for the continue-time antenna system, as shown in Figure 5. Particularly, the feedback control loop consists of the antenna self-movement dynamics and the antenna heading controller. Then, the antenna heading controller can be designed as

$$\tau^*_i(k) = \underbrace{k_1[\gamma^*_i(k) - \theta^*_i(k)]}_{P \text{ control}} - \underbrace{k_2(\Delta\theta^*_i(k))}_{D \text{ control}} \quad (28)$$

where $k_1 \in \mathcal{R}^+$ and $k_2 \in \mathcal{R}^+$ are the proportional gain and differential gain, respectively. $\Delta\theta^*_i(k) = [\theta^*_i(k) - \theta^*_i(k-1)]/\delta$ is the actual self-movement angle velocity.

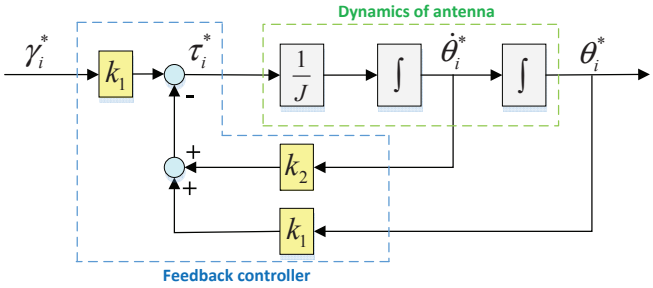

Fig. 5: Feedback control loop for the antenna heading control.

Equation (28) is driven by the difference between the desired self-movement angle γ^*_i and the actual self-movement angle θ^*_i, and the differential of θ^*_i. These results produce the torque τ^*_i to steer the antenna to certain self-movement angle γ^*_i.

Remark 3: This paper focuses on using heading control to establish a robust communication channel for the two UAVs. However, in some emergency scenarios, the communication links between two UAVs cannot be always guaranteed. Alternatively, a group of UAVs are demanded to relay the data. In such case, some communication-related issues need to be studied, such as if phase array antenna should be used, the switching between multiple directions, and practical ways to maintaining path lifetime of multiple links. Nevertheless, the results developed in this paper still apply for each communication link within a multiple-UAV network.

This article has been accepted for publication in a future issue of this journal, but has not been fully edited. Content may change prior to final publication. Citation information: DOI 10.1109/JIOT.2018.2875428, IEEE Internet of Things Journal

V. Performance Analysis

A. Convergence Conditions for the Estimation Algorithm

We investigate the boundedness of estimation error for the consensus-based UKF algorithm. With the linearization method in [45], [47], RSSI measurement (8) for UAV i is

$$z_{R,i}(k) = \mathcal{H}_R(k)X(k) + \varpi_{R,i}(k) \tag{29}$$

where $\mathcal{H}_R(k)$ is defined as $\frac{\partial z_{R,i}(k)}{\partial X(k)}\big|_{X(k|k-1)}$, i.e., $\mathcal{H}_R(k) = [-\frac{\partial \gamma_j(k)}{2\partial x_i(k)}K_{t,j}\sin(\gamma_j(k) - \theta_j(k)) - \frac{\partial \gamma_i(k)}{2\partial x_i(k)}K_{r,i}\sin(\gamma_i(k) - \theta_i(k)) - \frac{\partial L_f}{\partial x_i(k)}, -\frac{\partial \gamma_j(k)}{2\partial y_i(k)}K_{t,j}\sin(\gamma_j(k) - \theta_j(k)) - \frac{\partial \gamma_i(k)}{2\partial y_i(k)}K_{r,i}\sin(\gamma_i(k) - \theta_i(k)) - \frac{\partial L_f}{\partial y_i(k)}, 0, 0, 0, 0, \frac{1}{2}K_{r,i}\sin(\gamma_i(k) - \theta_i(k)), -\frac{\partial \gamma_j(k)}{2\partial x_j(k)}K_{t,j}\sin(\gamma_j(k) - \theta_j(k)) - \frac{\partial \gamma_i(k)}{2\partial x_j(k)}K_{r,i}\sin(\gamma_i(k) - \theta_i(k)) - \frac{\partial L_f}{\partial x_j(k)}, -\frac{\partial \gamma_j(k)}{2\partial y_j(k)}K_{t,j}\sin(\gamma_j(k) - \theta_j(k)) - \frac{\partial \gamma_i(k)}{2\partial y_j(k)}K_{r,i} \times \sin(\gamma_i(k) - \theta_i(k)) - \frac{\partial L_f}{\partial y_j(k)}, 0, 0, 0, 0, \frac{1}{2}K_{t,j}\sin(\gamma_j(k) - \theta_j(k))]$.

The cross-covariance matrix between last estimate and current prediction is defined, i.e.,

$$\begin{aligned} P_{i,\hat{X}(k-1)\hat{X}(k|k-1)} &= \textstyle\sum_{s=0}^{2L} W_s[\mathcal{X}_s(k-1) - \hat{X}(k-1)] \\ &\quad \times [\mathcal{X}_s(k\,|k-1) - \hat{X}(k\,|k-1)]^T. \end{aligned}$$

Accordingly, a pseudo system matrix $\mathcal{F}(k)$ is approximated as $\mathcal{F}(k) \triangleq P^T_{i,\hat{X}(k-1)\hat{X}(k|k-1)}P^{-1}(k-1)$. Thus, Equation (5) can be rewritten as $X(k+1) = \mathcal{F}(k)X(k) + V(k)$, and the modified predicted error covariance $P(k|k-1)$ is updated as

$$P(k|k-1) = \mathcal{F}(k)P(k-1)\mathcal{F}^T(k) + Q(k-1). \tag{30}$$

Through the linearization of measurement $z_{R,i}(k)$, one has

$$\begin{aligned} & P_{i,\hat{X}(k)\hat{z}_{R,i}(k)} \\ &= \int [X(k) - \hat{X}(k)][z_{R,i}(k) - \hat{z}_{R,i}(k)]^T \mathcal{N}_{es} dX(k) \\ &= \int [X(k) - \hat{X}(k)][\mathcal{H}_R(k)X(k) + \varpi_{R,i}(k) \\ &\quad -\mathcal{H}_R(k)\hat{X}(k)]^T \mathcal{N}_{es} dX(k) \\ &= P(k\,|k-1\,)\mathcal{H}_R^T(k), \end{aligned} \tag{31}$$

where $\mathcal{N}_{es}$ is probability density for estimation. For symmetry property, one has $\mathcal{H}_R(k) = P^T_{i,\hat{X}(k)\hat{z}_{R,i}(k)}P^{-1}(k\,|k-1\,)$.

Based on (31) and noting with the property of $P_{i,\hat{z}_{R,i}(k)\hat{z}_{R,i}(k)} = \mathcal{H}_R(k)P(k\,|k-1)\mathcal{H}_R^T(k) + R_{R,i}(k)$, Equation (25) can be rearranged as

$$\begin{aligned} \mathcal{K}_{R,i}(k) &= P(k\,|k-1)\mathcal{H}_R^T(k)[\mathcal{H}_R(k) \\ &\quad \times P(k\,|k-1)\mathcal{H}_R^T(k) + R_{R,i}(k)]^{-1} \\ P_R(k) &= P(k\,|k-1) - P(k\,|k-1)\mathcal{H}_R^T(k) \\ &\quad \times P^{-1}_{i,\hat{z}_{R,i}(k)\hat{z}_{R,i}(k)}P_{i,\hat{z}_{R,i}(k)\hat{z}_{R,i}(k)}\mathcal{K}_{R,i}^T(k) \\ &= (I - \mathcal{K}_{R,i}(k)\mathcal{H}_R(k))P(k\,|k-1). \end{aligned} \tag{32}$$

Similarly, Equation (23) and (24) can be updated as

$$\begin{aligned} \mathcal{K}_{G,i}(k) &= P(k\,|k-1)(H^{\#}_{G,i}(k))^T[H^{\#}_{G,i}(k) \\ &\quad \times P(k\,|k-1)(H^{\#}_{G,i}(k))^T + R_{G,i}(k)]^{-1} \\ P_G(k) &= (I - \mathcal{K}_{G,i}(k)H^{\#}_{G,i}(k))P(k\,|k-1). \end{aligned} \tag{33}$$

Substituting (32) and (33) into (27), we have

$$\begin{aligned} P(k) &= P(k|k-1) - \alpha_G\mathcal{K}_{G,i}(k)H^{\#}_{G,i}(k)P(k|k-1) \\ &\quad -\alpha_R\mathcal{K}_{R,i}(k)\mathcal{H}_R(k)P(k|k-1) \\ &= [I - \alpha_G\mathcal{K}_{G,i}(k)H^{\#}_{G,i}(k) - \alpha_R\mathcal{K}_{R,i}(k) \\ &\quad \times\mathcal{H}_R(k)]P(k|k-1). \end{aligned} \tag{34}$$

Define the prediction and estimation errors as $\tilde{X}(k+1\,|k\,) = X(k+1) - \hat{X}(k+1\,|k\,)$ and $\tilde{X}(k) = X(k) - \hat{X}(k)$, respectively. Inspired by the idea in [44], the following theorem is given to illustrate the effectiveness of update rules (26) and (27).

Theorem 1: Consider state model (5) with the update rules (26) and (27). If these exist real numbers $h_{\min}$, $f_{\min}$ and $h_{\max}$, $f_{\max}$, positive real constants $p_{\min}$, $q_{\min}$, $r_{\min}$ and $p_{\max}$, $q_{\max}$, $r_{\max}$, such that the following conditions hold, i.e., (a): $p_{\min}I \le P(k) \le p_{\max}I$, $q_{\min}I \le Q(k) \le q_{\max}I$, $r_{\min}I \le R^{\#}_{G,i}(k) \le r_{\max}I$, $r_{\min}I \le R_{R,i}(k) \le r_{\max}I$; (b): $h^2_{\min}I \le H^{\#}_{G,i}(k)(H^{\#}_{G,i}(k))^T \le h^2_{\max}I$, $h^2_{\min}I \le \mathcal{H}_R(k)\mathcal{H}_R^T(k) \le h^2_{\max}I$, $f^2_{\min}I \le \mathcal{F}(k)\mathcal{F}^T(k) \le f^2_{\max}I$, then the estimation error $\tilde{X}(k)$ is bounded.

Proof: The proof can be found in Appendix A. ■

B. Cramér-Rao Lower Bound for the Estimation Algorithm

We drive the Cramér-Rao Lower Bound (CRLB) for the proposed algorithm. CRLB is a lower bound to the error variance of any parameter estimation, which serves as an important tool in the performance evaluation of estimation.

Let $\mathcal{X}(k) = \{X(0), X(1), ..., X(k)\}$ represent state vector series, and $\mathcal{Z}(k) = \{z(1), z(2), ..., z(k)\}$ is the observation value, where $z(k) \in \{z^{\#}_{G,i}(k), z_{R,i}(k)\}$. In addition, it is defined that $R(k) \in \{R^{\#}_{G,i}(k), R_{R,i}(k)\}$ and $\mathcal{H}(k) \in \{H^{\#}_{G,i}(k), \mathcal{H}_R(k)\}$. $p(\mathcal{Z}(k), \mathcal{X}(k))$ is the joint probability density of the pair $(\mathcal{Z}(k), \mathcal{X}(k))$. Then, the Fisher information matrix is given as

$$\mathcal{J}(k) = -E[\tfrac{\partial^2 \ln p(\mathcal{Z}(k),\mathcal{X}(k))}{\partial X^2(k)}]. \tag{35}$$

As such, the estimation error of CRLB can be defined as

$$\mathcal{P}(k) \triangleq E\{[X(k) - \hat{X}(k)][X(k) - \hat{X}(k)]^T\} \geqslant \mathcal{J}^{-1}(k). \tag{36}$$

With [45], the sequence $\{\mathcal{J}(k)\}$ of posterior information matrices for estimating state $\{X(k)\}$ obeys the recursion

$$\mathcal{J}(k) = \mathcal{L}_{2,2}(k) - \mathcal{L}_{2,1}(k)[\mathcal{J}(k-1) + \mathcal{L}_{1,1}(k)]^{-1}\mathcal{L}_{1,2}(k), \tag{37}$$

with

$$\begin{aligned} \mathcal{L}_{1,1}(k) &= -E\left\{\tfrac{\partial^2 \ln p(X(k)|X(k-1))}{\partial X^2(k-1)}\right\} \\ \mathcal{L}_{1,2}(k) &= -E\left\{\tfrac{\partial^2 \ln p(X(k)|X(k-1))}{\partial X(k)\partial X(k-1)}\right\} \\ \mathcal{L}_{2,1}(k) &= -E\left\{\tfrac{\partial^2 \ln p(X(k)|X(k-1))}{\partial X(k-1)\partial X(k)}\right\} \\ \mathcal{L}_{2,2}(k) &= -E\left\{\tfrac{\partial^2 \ln p(X(k)|X(k-1))}{\partial X^2(k)} + \tfrac{\partial^2 \ln p(z(k)|X(k))}{\partial X^2(k)}\right\}. \end{aligned}$$

Thereby, the following corollary is given to show the CRLB.

This article has been accepted for publication in a future issue of this journal, but has not been fully edited. Content may change prior to final publication. Citation information: DOI 10.1109/JIOT.2018.2875428, IEEE Internet of Things Journal

TABLE II: Parameter values used in the simulation.

Parameter	Value	Parameter	Value
l	0.2	K_1	0.01
m	2	K_2	0.01
g	9.8	K_3	0.01
I_1	1.25	K_4	0.012
I_2	1.25	K_5	0.012
I_3	2.5	K_6	0.012
$k_{i,z1}$	40	$k_{i,z2}$	10
$k_{i,\varphi 1}$	30	$k_{i,\varphi 2}$	7
$k_{i,\psi 1}$	30	$k_{i,\psi 2}$	7
δ	$0.1s$	$P_{t,i}\|$dBm	20|dBm
$G_{t,i}^{\max}\|$dBm	10|dBm	$G_{t,i}^{\min}\|$dBm	-10|dBm
$q_{G,\max}$	600	$q_{RS,\max}$	1100

Corollary 1: Applying the UKF algorithm to DAAN system, the CRLB can be calculated as

$$\mathcal{P}(k) \geqslant \mathcal{J}^{-1}(k), \tag{38}$$

where the Fisher information matrix $\mathcal{J}(k)$ is defined by

$$\begin{aligned}\mathcal{J}(k) \quad = \quad & Q^{-1}(k) + \mathcal{H}^T(k)R^{-1}(k)\mathcal{H}(k) - Q^{-1}(k)\mathcal{F}(k) \\ & \times[\mathcal{J}(k-1)+\mathcal{F}^T(k)Q^{-1}(k)\mathcal{F}(k)]^{-1}\mathcal{F}^T(k)Q^{-1}(k),\end{aligned}$$

and $\mathcal{J}(0)$ can be calculated by the inverse of initial covariance matrix $P(0)$, i.e., $\mathcal{J}(0) = P^{-1}(0)$.

Proof: The proof is given in Appendix B. ■

C. Performance Metrics for the Heading Controller

In this section, we give the performance metrics for the heading controller (28). Referring to the knowledge of discrete-data control system [46], the closed-loop pulse transfer function $\bar{G}(\mathbf{z})$ in Figure 5 is given as

$$\bar{G}(\mathbf{z}) = \frac{k_1 G(\mathbf{z})}{1 + k_1 G(\mathbf{z})}, \tag{39}$$

where $G(\mathbf{z})$ denotes the open-loop transfer function, and symbol $\mathbf{z}$ represents a complex variable.

In the following, the performance metrics are presented.

Theorem 2: Consider the closed-loop system (39) with heading controller (28). Suppose that the parameters are chosen such that $J > 0$, $k_2 > 0$, $2 + 2e^{-k_2\delta/J} - k_1/k_2 + (k_1/k_2)e^{-k_2\delta/J} > 0$ and $k_1 < (2k_2(1 + e^{-k_2\delta/J}))/(1 - e^{-k_2\delta/J})$, then the close-loop system is asymptotically stable, i.e., $\theta_i(k) \to \gamma_i(k)$ with a limited time interval.

Proof: The proof is given in Appendix C. ■

VI. Simulation Results

Simulation results are presented in this section. Some parameters used in simulation are given by Table II. Particularly, the initial states of two UAVs are given as: $X_1(0) = [0\text{m}, 0\text{m}, 0\text{m}, \pi/36\text{rad}, \pi/24\text{rad}, 0\text{rad}, 6\text{rad}]^T$ and $X_2(0) = [-300\text{m}, -300\text{m}, -200\text{m}, \pi/12\text{rad}, \pi/24\text{rad}, 0\text{rad}, 6\text{rad}]^T$.

1) Height and Angles Tracking for UAV 1

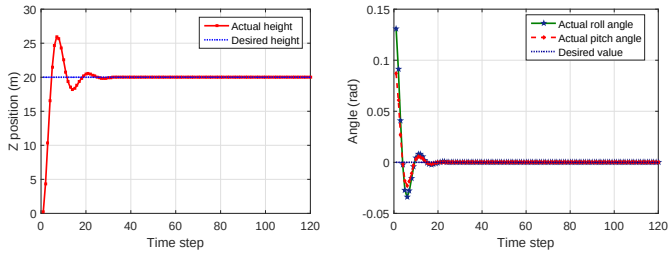

(a) Height tracking. (b) Angles tracking.

Fig. 6: Height and angles of UAV 1 with the tracking controller.

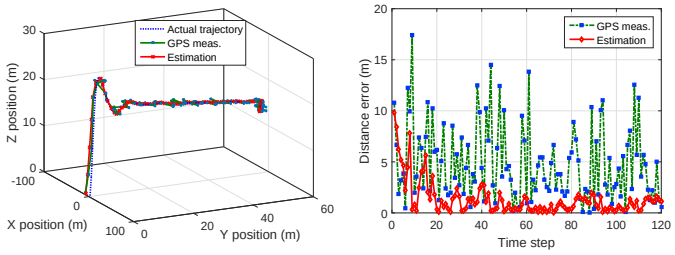

(a) Trajectories of UAV 1. (b) Distance errors for UAV 1.

Fig. 7: Trajectories and errors of UAV 1 with GPS measurements.

To test the PD-based tracking controller in Section IV-A, the desired height of UAV 1 is set as 20m, i.e., UAV 2 is assumed to be static in the air during the simulation process. In addition, the desired pitch and roll angles of UAV 1 are set as zeros. As such, the actual height of UAV 1 is shown in Figure 6(a), while the actual pitch and roll angles of UAV 1 are shown in Figure 6(b). Clearly, the heights, pitch and roll angles can reach to the desired value with a limited time interval.

2) Self-position Estimation for UAV 1

In this section, we test the self-position estimation algorithm as given in Section IV-B. The actual, measured and estimated trajectories of UAV 1 are depicted in Figure 7(a). It is noted that the proposed UKF-based algorithm can well

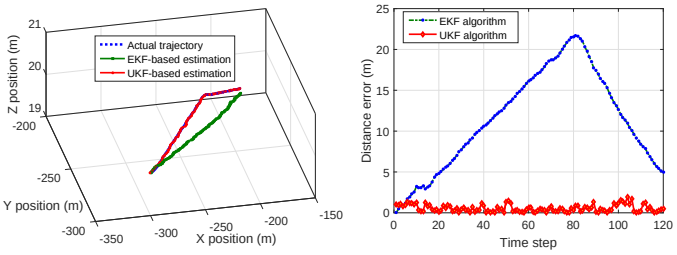

(a) Actual and estimated trajectories. (b) Distance errors.

Fig. 8: Comparison with EKF and UKF algorithms for UAV 2.

This article has been accepted for publication in a future issue of this journal, but has not been fully edited. Content may change prior to final publication. Citation information: DOI 10.1109/JIOT.2018.2875428, IEEE Internet of Things Journal

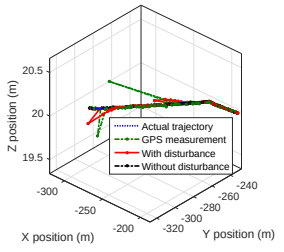

(a) Trajectories when only GPS is available.

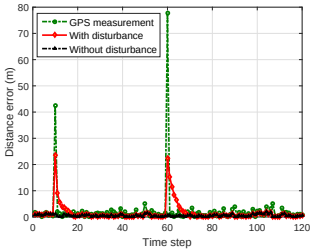

(b) Distance errors when only GPS is available.

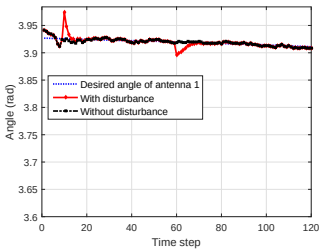

(c) Angles of antenna 1 with GPS measurement.

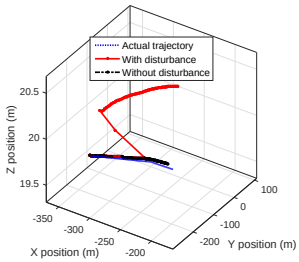

(d) Trajectories when only RSSI is available.

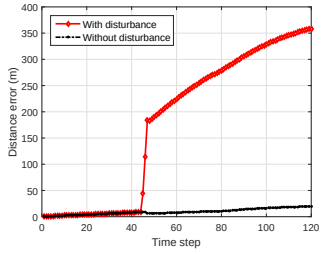

(e) Distance errors when only RSSI is available.

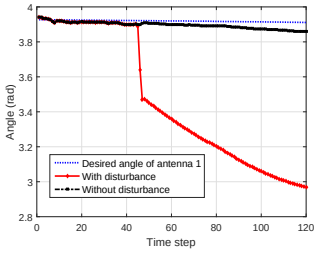

(f) Angles of antenna 1 with RSSI measurement.

Fig. 9: Trajectories, distance errors and heading directions without fusion.

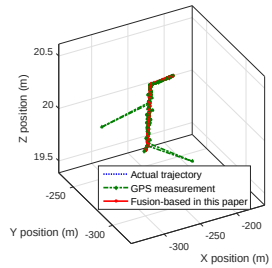

(a) Trajectories of UAV 2 in this paper.

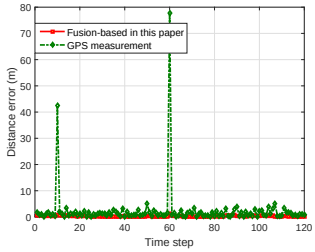

(b) Distance errors of UAV 2 in this paper.

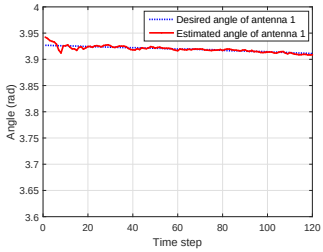

(c) Angles of antenna 1 in this paper.

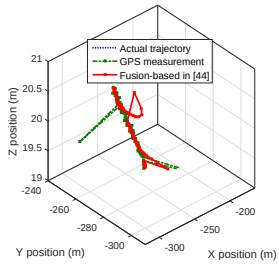

(d) Trajectories of UAV 2 with [44].

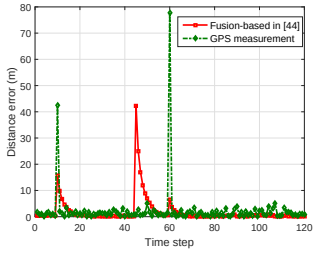

(e) Distance errors of UAV 2 with [44].

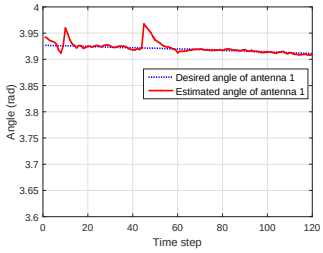

(f) Angles of antenna 1 with stochastic weights.

Fig. 10: Trajectories, distance errors and heading directions with consensus-based fusion.

estimate the self-position for UAV 1. To show more clearly, the distance errors for GPS measurements are defined as $\text{error}_1(k) = [(x_1(k) - z_{G,1,1}(k))^2 + (y_1(k) - z_{G,1,2}(k))^2 + (z_1(k) - z_{G,1,3}(k))^2]^{0.5}$. Similarly, the distance errors for UKF-based estimation are defined as $\text{error}_2(k) = [(x_1(k) - \hat{x}_1(k))^2 + (y_1(k) - \hat{y}_1(k))^2 + (z_1(k) - \hat{z}_1(k))^2]^{0.5}$. The distance errors are shown in Figure 7(b). Clearly, the proposed UKF-based algorithm can reduce the influence of noise.

3) Comparison with EKF and UKF Algorithms for UAV 2

As mentioned in Section IV-B, the conventional Kalman filtering is not applicable for the nonlinear model. Although EKF has been developed to address the nonlinearity [41], the accuracy of EKF is limited due to the approximation of nonlinear model. Then, we adopt EKF and UKF separately to estimate the position of UAV 2. As such, the actual and estimated trajectories of UAV 2 are shown in Figure 8(a). Correspondingly, the distance errors are shown in Figure 8(b). It is obvious that UKF algorithm in this paper can guarantee the estimation accuracy as compared with EKF algorithm [41].

4) Consensus-based UKF Algorithm for UAV 2

To verify the performance of consensus-based UKF algorithm, three cases are considered in this section. Case 1: only GPS signals are available to UAV 1; Case 2: only RSSI signals are available to UAV 1; Case 3: GPS and RSSI are both available.

In Case 1, we consider two subcases. Case 1(a): There is no malicious data on GPS measurements, i.e., the GPS measurements are always trusted. Case 1(b): Malicious data attacks the measurements, e.g., malicious GPS measurements are added at time steps $k = 10$ and $k = 60$. Under Case 1(a) and Case 1(b), the actual, measured and estimated trajectories of UAV 2 are shown in Figure 9(a). Moreover, the distance errors are shown in Figure 9(b), and the estimated angles of directional antenna 1 are shown in Figure 9(c). Under Case 2, malicious RSSI measurements are added at time step $k = 45$. The actual, measured and estimated trajectories of UAV

This article has been accepted for publication in a future issue of this journal, but has not been fully edited. Content may change prior to final publication. Citation information: DOI 10.1109/JIOT.2018.2875428, IEEE Internet of Things Journal

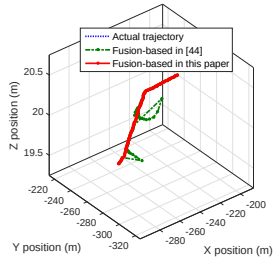

(a) Trajectories of UAV 2.

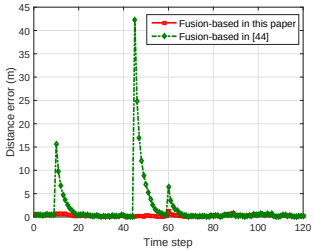

(b) Comparison of the distance errors.

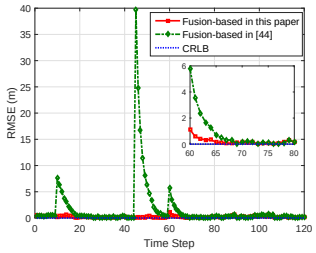

(c) RMSE vs. CRLB.

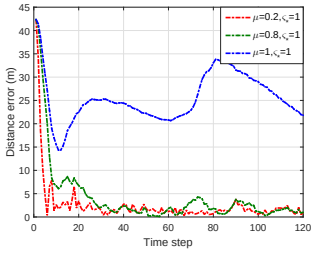

(d) Convergence time with different measurement covariances.

Fig. 11: RMSE of distance errors vs. CRLB and convergence time with different measurement covariances.

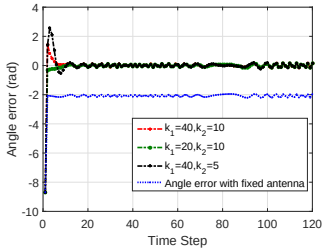

(a) Angle errors Scenario 1.

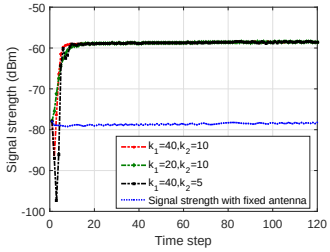

(b) Signal strength Scenario 1.

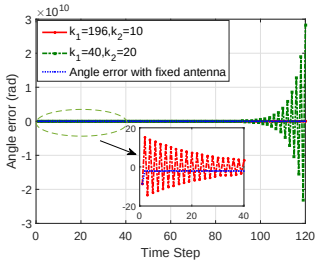

(c) Angle errors in Scenario 2.

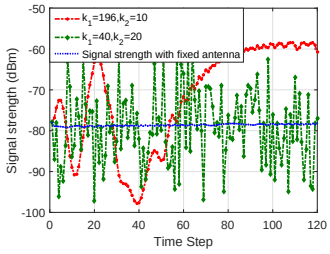

(d) Signal strength in Scenario 2.

Fig. 12: Performance comparison with and without heading control.

2 are shown in Figure 9(d), the distance errors are given in Figure 9(e), and the estimated angles of directional antenna 1 are described in Figure 9(f). It it obvious that the malicious GPS (or RSSI) measurements reduce the estimation accuracy of UAV 2. In order to reduce the influence of malicious measurements, we use consensus-based UKF algorithm to estimate the position of UAV 2 in Case 3. Similar to Case 1 and Case 2, the actual, measured and estimated trajectories of UAV 2 are shown in Figure 10(a). Correspondingly, the distance errors are shown in Figure 10(b), and the estimated angles of directional antenna 1 are described in Figure 10(c). Clearly, the effect of malicious GPS and RSSI measurements can be relaxed with the consensus-based UKF algorithm in this paper. This comparative study shows that the fusion of measurements is important, and the consensus-based UKF algorithm developed in this paper is meaningful.

To test the advantage of deterministic weights in our algorithm, we give the results with stochastic weights for the consensus-based UKF algorithm [44]. Under stochastic weights, the actual, measured and estimated trajectories of UAV 2 are shown in Figure 10(d), while the the distance errors are given in Figure 10(e). Moreover, the estimated angles of directional antenna 1 are described in Figure 10(f). Comparing with the stochastic weights as given in [44], the deterministic weights in this paper, shown in Figures 11(a) and Figure 11(b), can reduce the impact of malicious measurements, as it maximizes the contributions of stable measurements while minimizing the contributions of those that are less stable. Of interest, at the moments of malicious measurements, $\alpha_G(10) = 0.0276, \alpha_R(10) = 0.9724$, $\alpha_G(45) = 0.8969, \alpha_R(45) = 0.1031$ and $\alpha_G(60) = 0.0848$, $\alpha_R(60) = 0.9152$.

In order to illustrate the lower bound of the consensus-based UKF algorithm, we define the RMSE, i.e., root mean square error. The RMSE is calculated by averaging the square error between $x(k)$ and $\hat{x}(k)$, where $\hat{x}(k)$ is the estimated values by different localization algorithms. The error performance of the two methods is compared with the theoretically derived CRLB, which is calculated by using (38). Particularly, the initial information matrix for computation of the CRLB is set as $\mathcal{J}(0) = P^{-1}(0)$. From Figures 11(c), the estimation accuracy by consensus-based UKF algorithm with deterministic fusion in this paper is closest to the theoretical CRLB.

5) Simulation for Antenna Heading Controller

Moreover, we test the overall performance of the antenna control algorithm that integrates tracking, fusion and the local feedback controller designed in Section IV-D. Particularly, the heading direction errors are defined as $\theta_{err1}(k) = \gamma_1(k) - \theta_1(k)$ and $\theta_{err2}(k) = \gamma_2(k) - \theta_2(k)$. For comparison, two scenarios are presented. In Scenario 1, the controller gains satisfy the stability condition in Theorem 2. In Scenario 2, the controller gains do not satisfy the stability condition. Then, the proportional and derivative gains in Scenario 1 are set as: $k_1 = 20$, $k_2 = 10$; $k_1 = 40$, $k_2 = 10$; $k_1 = 40$, $k_2 = 5$. On the other side, the proportional and derivative gains in Scenario 2 are set as: $k_1 = 196$, $k_2 = 10$; $k_1 = 40$, $k_2 = 20$. With heading controller (28), the angle errors of antenna 1 in Scenario 1 are depicted by Figure 12(a), while the signal strengths of communication channel are shown by Figure 12(b). It is obvious that, a high proportional gain results in a large change in the output for a given error change, and the derivative term has the effect of increasing the stability, reducing the

overshoot, and improving the transient response. Meanwhile, the angle errors in Scenario 2 are depicted by Figure 12(c), while the signal strengths are shown by Figure 12(d). Clearly, the signal strength in Scenario 1 can be improved and the angle errors can be reduced. The above results also verify the importance and meaning of the stability condition in Theorem 2. Besides, this comparative study shows that with heading control in this paper is significative.

6) Convergence Time for Consensus-based UKF Algorithm

As it is pointed in [49], the high value of measurement covariance matrix (e.g., $R_{G,i}$) leads to a slow convergence rate of EKF algorithm, while a slow value leads to a fast convergence rate. Meanwhile, the UKF algorithm converges faster than the one of EKF algorithm [49]. Based on these propositions, we believe that the convergence time of consensus-based UKF algorithm is highly related with the measurement covariance matrix. In order to verify this conclusion, we set different $R_{G,i}$, which is given as $R_{G,i}(k+1) = \mu P_{i,\hat{z}_{R,i}(k)\hat{z}_{R,i}(k)} + \varsigma_* I$, where $\mu > 0$ and $\varsigma_* > 0$ are weights. Correspondingly, the convergence processes are shown in Figure 11(d). It is obvious that a slow value of $R_{G,i}$ leads to a fast convergence rate.

VII. Conclusions and Future Works

In this paper, we investigate the RSSI-based heading control problem for robust long-range aerial communication in UAV networks. Specifically, an integrated model that consists of UAV dynamics, directional antenna dynamics, GPS measurements and RSSI measurements is constructed. Based on the integrated model, a PD-based tracking controller is designed for UAV to ensure the consistency of heights, pitch and roll angles, wherein the UAV dynamics have nonlinear property with six freedoms. As such, we develop a consensus-based UKF algorithm to estimate the position of UAVs. Through consensus fusion, the influence of malicious measurements is reduced, and the signal strength can be improved by comparing with the omni-directional antenna based works. Moreover, the convergence conditions and Cramé-Rao lower bounds are also provided. Finally, simulation results are given to show the effectiveness of the proposed approach.

In future, we will pursue field testing, and also consider the case of communication failure. Moreover, how to extend the framework to a group of UAVs is also our future work.

Appendix A
Proof of Theorem 1

The Lyapunov function is given as

$$\mathcal{V}(\tilde{X}(k{+}1\,|k\,)){=}\,\tilde{X}^T(k{+}1\,|k\,)P^{-1}(k{+}1\,|k\,)\tilde{X}(k{+}1\,|k\,). \quad (40)$$

Based on (40) and the condition (a) in Theorem 1, we have

$$\frac{\left\|\tilde{X}(k+1|k)\right\|^2}{p_{\max}} \le \mathcal{V}(\tilde{X}(k{+}1\,|k\,)) \le \frac{\left\|\tilde{X}(k+1|k)\right\|^2}{p_{\min}}. \quad (41)$$

From (24), (25) and (26), we have

$$\begin{aligned}\tilde{X}(k{+}1\,|k\,) &= X(k+1) - \hat{X}(k+1|k)\\ &= X(k) - \hat{X}(k\,|k{-}1\,) - \alpha_G\mathcal{K}_{G,i}(k)(z^{\#}_{G,i}(k)\\ &\quad -\hat{z}^{\#}_{G,i}(k\,|k{-}1\,)) - \alpha_R\mathcal{K}_{R,i}(k)(z_{R,i}(k)\\ &\quad -\hat{z}_{R,i}(k\,|k{-}1\,)) + V(k). \quad (42)\end{aligned}$$

Substituting (7) and (29) into (42), we have

$$\begin{aligned}&\tilde{X}(k{+}1\,|k\,)\\ =\;& (I - \alpha_G\mathcal{K}_{G,i}(k)H^{\#}_{G,i}(k) - \alpha_R\mathcal{K}_{R,i}(k)\\ &\times\mathcal{H}_R(k))\tilde{X}(k|k{-}1) + \{-\alpha_G\mathcal{K}_{G,i}(k)\varpi^{\#}_{G,i}(k)\\ &-\alpha_R\mathcal{K}_{R,i}(k)\varpi_{R,i}(k)\} + V(k). \quad (43)\end{aligned}$$

Of note, we define $\Upsilon{=}\{G,R\}$, $\omega_{G,i}(k) = \varpi^{\#}_{G,i}(k)$, $\omega_{R,i}(k) = \varpi_{R,i}(k)$ and $\mathcal{H}_G(k) = H^{\#}_{G,i}(k)$ to simplify the proof. Equation (43) is hence rearranged as

$$\begin{aligned}&\tilde{X}(k{+}1\,|k\,)\\ =\;& [I{-}\textstyle\sum_{\xi\in\Upsilon}\alpha_\xi\mathcal{K}_{\xi,i}(k)\mathcal{H}_\xi(k)]\tilde{X}(k\,|k{-}1)\\ &+\textstyle\sum_{\xi\in\Upsilon}[-\alpha_\xi\mathcal{K}_{\xi,i}(k)\omega_{\xi,i}(k)] + V(k). \quad (44)\end{aligned}$$

Similarly, Equation (34) can be expressed as

$$P(k) = [I{-}\textstyle\sum_{\xi\in\Upsilon}\alpha_\xi\mathcal{K}_{\xi,i}(k)\mathcal{H}_\xi(k)]P(k|k{-}1). \quad (45)$$

Denoting $\Gamma = I{-}\sum_{\xi\in\Upsilon}\alpha_\xi\mathcal{K}_{\xi,i}(k)\mathcal{H}_\xi(k)$ and substituting (44) into (40), one has

$$\begin{aligned}&E\{\mathcal{V}(\tilde{X}(k{+}1\,|k\,))\,\Big|\tilde{X}(k\,|k{-}1\,)\,\}\\ =\;& E\{\tilde{X}^T(k{+}1\,|k\,)P^{-1}(k+1\,|k\,)\tilde{X}(k{+}1\,|k\,)\,\Big|\tilde{X}(k\,|k{-}1\,)\,\}\\ =\;& \Phi_X(k+1) + \Phi_{G+R}(k+1) + \Phi_V(k+1)\end{aligned}$$

where $\Phi_X(k+1) = E\{(\Gamma\tilde{X}(k|k-1))^TP^{-1}(k+1|k)\Gamma\tilde{X}(k|k-1))|\tilde{X}(k|k{-}1)\}$, $\Phi_{G+R}(k+1) = E\{[\sum_{\xi\in\Upsilon} -\alpha_\xi\mathcal{K}_{\xi,i}(k)\omega_{\xi,i}(k)]^TP^{-1}(k+1\,|k\,)[\sum_{\xi\in\Upsilon}-\alpha_\xi\mathcal{K}_{\xi,i}(k)\omega_{\xi,i}(k)]\,|\tilde{X}(k\,|k{-}1\,)\,\}$ and $\Phi_V(k+1) = E\{V^T(k)P^{-1}(k+1|k)V(k)\,|\tilde{X}(k|k{-}1)\}$.

It is noted that $P(k{+}1\,|k\,) = \int[X(k){-}\hat{X}(k{+}1\,|k\,)][X(k){-}\hat{X}(k+1\,|k\,)]^T\mathcal{N}_{X(k)}dX(k) + Q(k)$ and $P(k) = \int[X(k) - \hat{X}(k+1\,|k\,)][X(k) - \hat{X}(k+1\,|k\,)]^T\mathcal{N}_{X(k)}dX(k)$. Hence, we can obtain the relationship between $P(k{+}1\,|k\,)$ and $P(k)$, i.e., $P^{-1}(k+1\,|k\,) = [P(k) + Q(k)]^{-1}$, where $\mathcal{N}_{X(k)}$ denotes the probability density for prediction. Based on this, it is obtained that $P^{-1}(k+1\,|k\,) \le P^{-1}(k)$.

For $\Phi_X(k{+}1)$, one has

$$\begin{aligned}&\Phi_X(k{+}1)\\ \le\;& E\{(\Gamma\tilde{X}(k|k-1))^TP^{-1}(k)(\Gamma\tilde{X}(k|k-1))|\tilde{X}(k|k{-}1)\}\\ \le\;& E\{\tilde{X}^T(k\,|k{-}1\,)[I - \textstyle\sum_{\xi\in\Upsilon}\alpha_\xi\mathcal{K}_{\xi,i}(k)\mathcal{H}_\xi(k)]^T\\ &\times P^{-1}(k|k-1)\tilde{X}(k\,|k\text{-}1\,)\,\Big|\tilde{X}(k\,|k\text{-}1)\,\}\\ \le\;& E\{\tilde{X}^T(k|k{-}1)P^{-1}(k|k-1)\tilde{X}(k\,|k-1\,)|\tilde{X}(k|k{-}1)\}\\ \le\;& E\{\mathcal{V}(\tilde{X}(k\,|k{-}1))\}. \quad (46)\end{aligned}$$

For $\Phi_{G+R}(k+1)$, denoting $\bar{R}(k) = \sum_{\xi\in\Upsilon}(\alpha_\xi\omega_{\xi,i}(k))^2$, and then one has

$$\begin{aligned}
&\Phi_{G+R}(k+1)\\
\leq\ & E\{[-\textstyle\sum_{\xi\in\Upsilon}\alpha_\xi\mathcal{K}_{\xi,i}(k)\omega_{\xi,i}(k)]^T P^{-1}(k)\\
&\times[-\textstyle\sum_{\xi\in\Upsilon}\alpha_\xi\mathcal{K}_{\xi,i}(k)\omega_{\xi,i}(k)]\Big|\tilde{X}(k\,|k-1)\,\}\\
\leq\ & p_{\min}^{-1}E\{[-\textstyle\sum_{\xi\in\Upsilon}\alpha_\xi\mathcal{K}_{\xi,i}(k)\omega_{\xi,i}(k)]^T\\
&\times[-\textstyle\sum_{\xi\in\Upsilon}\alpha_\xi\mathcal{K}_{\xi,i}(k)\omega_{\xi,i}(k)]\Big|\tilde{X}(k\,|k-1)\,\}\\
\leq\ & p_{\min}^{-1}E\{\textstyle\sum_{\xi\in\Upsilon}(\alpha_\xi\omega_{\xi,i}(k))^2\mathcal{K}_{\xi,i}^T(k)\\
&\times\mathcal{K}_{\xi,i}(k)\Big|\tilde{X}(k\,|k-1)\,\}\\
\leq\ & p_{\min}^{-1}\bar{R}(k)E\{\textstyle\sum_{\xi\in\Upsilon}[\mathcal{K}_{\xi,i}^T(k)\mathcal{K}_{\xi,i}(k)]\Big|\tilde{X}(k\,|k-1)\,\}.
\end{aligned}$$

In view of condition (b) and (30), we have $(p_{\min}f_{\min}^2 + q_{\min})I \leq P(k|k-1) \leq (p_{\max}f_{\max}^2 + q_{\max})I$. Define $k_{\max} = \frac{(p_{\max}f_{\max}^2+q_{\max})h_{\max}}{(p_{\min}f_{\min}^2+q_{\min})h_{\min}^2+r_{\min}}$, and then we have

$$\begin{aligned}
\mathcal{K}_{\xi,i}(k) &= \frac{P(k\,|k-1)\mathcal{H}_\xi^T(k)}{\mathcal{H}_\xi(k)P(k\,|k-1)\mathcal{H}_\xi^T(k)+R_{\xi,i}(k)}\\
&\leq \frac{(p_{\max}f_{\max}^2+q_{\max})h_{\max}}{(p_{\min}f_{\min}^2+q_{\min})h_{\min}^2+r_{\min}}I \leq k_{\max}I.
\end{aligned}$$

Moreover, $\Phi_{G+R}(k+1)$ is rearranged as $\Phi_{G+R}(k+1) \leq p_{\min}^{-1}\bar{R}(k)k_{\max}^2$.

For the $\Phi_V(k+1)$, one can obtain

$$\begin{aligned}
&\Phi_V(k+1)\\
\leq\ & E\{V^T(k)P^{-1}(k)V(k)\tilde{X}(k|k-1)\}\\
\leq\ & p_{\min}^{-1}Q(k) \leq p_{\min}^{-1}q_{\max}.
\end{aligned}$$

Thereby, we obtain the boundedness of prediction error, i.e,

$$\begin{aligned}
&E\{\mathcal{V}(\tilde{X}(k+1\,|k))\Big|\tilde{X}(k\,|k-1)\,\}\\
\leq\ & E\{\mathcal{V}(\tilde{X}(k\,|k-1))\} + p_{\min}^{-1}\bar{R}(k)k_{\max}^2 + p_{\min}^{-1}q_{\max}.
\end{aligned}$$

With these results, one has the boundedness of prediction error $E\{\mathcal{V}(\tilde{X}(k+1\,|k))\Big|\tilde{X}(k\,|k-1)\,\} - E\{\mathcal{V}(\tilde{X}(k\,|k-1))\}$. From (42), one has $\tilde{X}(k+1\,|k) = \tilde{X}(k) + V(k)$. As $V(k)$ is bounded, thus the estimation error $\tilde{X}(k)$ is also bounded.

APPENDIX B
PROOF OF COROLLARY 1

As the additive process noise is white Gaussian noise of zero mean, the conditional density function is expressed as

$$\begin{aligned}
&p(X(k)|X(k-1))\\
=\ & \frac{1}{\sqrt{2\pi|Q(k)|}}\exp\{-1/2[X(k)-\mathcal{F}(k-1)X(k-1)]^T\\
&\times Q^{-1}(k)[X(k)-\mathcal{F}(k-1)X(k-1)]\}
\end{aligned}$$

$$\begin{aligned}
&p(z(k)|X(k))\\
=\ & \frac{1}{\sqrt{2\pi|R(k)|}}\exp\{-1/2[z(k)-\mathcal{H}(k)X(k)]^T\\
&\times R^{-1}(k)[z(k)-\mathcal{H}(k)X(k)]\}.
\end{aligned}$$

With straightforward calculation, we have

$$\begin{aligned}
\mathcal{L}_{1,1}(k) &= \mathcal{F}^T(k)Q^{-1}(k)\mathcal{F}(k),\\
\mathcal{L}_{1,2}(k) &= -\mathcal{F}^T(k)Q^{-1}(k),\ \mathcal{L}_{2,1}(k) = -Q^{-1}(k)\mathcal{F}(k)\\
\mathcal{L}_{2,2}(k) &= Q^{-1}(k) + \mathcal{H}^T(k)R^{-1}(k)\mathcal{H}(k).
\end{aligned}$$

Thereby, the Fisher information matrix $\mathcal{J}(k)$ can be obtained by (35) and (37).

APPENDIX C
PROOF OF THEOREM 2

According to the relationship between the Laplace transform and the **z**-transform, the open-loop transfer function $G(\mathbf{z})$ for Figure 5 can be presented as follows

$$\begin{aligned}
G(\mathbf{z}) &= \mathbf{Z}\left[\tfrac{1}{\mathbf{s}(J\mathbf{s}+k_2)}\right] = \mathbf{Z}\left[\tfrac{1}{k_2}(\tfrac{1}{\mathbf{s}} - \tfrac{1}{\mathbf{s}+k_2/J})\right]\\
&= \tfrac{1}{k_2}\tfrac{(1-e^{-k_2\delta/J})\mathbf{z}}{(\mathbf{z}-1)(\mathbf{z}-e^{-k_2\delta/J})},
\end{aligned}$$

where $\mathbf{Z}[\cdot]$ represents **z**-transform and **s** represents a complex variable with real and imaginary parts.

In order to obtain the stability conditions of (39), the characteristic equation can be expressed as

$$\begin{aligned}
&1 + k_1G(\mathbf{z})\\
=\ & (\mathbf{z}-1)(\mathbf{z}-e^{-k_2\delta/J}) + \tfrac{k_1}{k_2}(1-e^{-k_2\delta/J})\mathbf{z}. \quad (47)
\end{aligned}$$

For the characteristic roots of the characteristic equation (47), we let $1 + k_1G(\mathbf{z}) = 0$ and $\mathbf{z} = (\vec{w}+1)/(\vec{w}-1)$, where $\vec{w}$ denotes a complex variable with real and imaginary parts. Through simplification, we have $(\frac{k_1}{k_2} - \frac{k_1}{k_2}e^{-k_2\delta/J})\vec{w}^2 + (2 - 2e^{-k_2\delta/J})\vec{w} + (2 + 2e^{-k_2\delta/J} - \frac{k_1}{k_2} + \frac{k_1}{k_2}e^{-k_2\delta/J}) = 0$.

According to the Routh stability criteria, the design parameters satisfy $J > 0$, $k_2 > 0$, $2 + 2e^{-k_2\delta/J} - k_1/k_2 + (k_1/k_2)e^{-k_2\delta/J} > 0$ and $k_1 < (2k_2(1+e^{-k_2\delta/J}))/(1-e^{-k_2\delta/J})$, the close-loop system is asymptotically stable, i.e., $\theta_i(k) \to \gamma_i(k)$ with a limited time interval.

REFERENCES

[1] L. Gupta, R. Jain, and G. Vaszkun, "Survey of important issues in UAV communication networks," *IEEE Commun. Surv. & Tutorials*, vol. 18, no. 2, pp. 1123-1152, May 2016.

[2] F. Koohifar, A. Kumbhar, and I. Guvenc, "Receding horizon multi-UAV cooperative tracking of moving RF source," *IEEE Commun. Lett.*, vol. 21, no. 6, pp. 1433-1436, Jun. 2017.

[3] H. Menouar, I. Guvenc, K. Akkaya, AS. Uluagac, A. Kadri, and A. Tuncer, "UAV-enabled intelligent transportation systems for the smart city: applications and challenges," *IEEE Commun. Mag.*, vol. 55, no. 3, pp. 22-28, Mar. 2017.

[4] M. Alzenad, A. El-Keyi, F. Lagum, and H. Yanikomeroglu, "3D placement of an unmanned aerial vehicle base station (UAV-BS) for energy-efficient maximal coverage," *IEEE Wirel. Commun. Lett.*, vol. 6, no. 4, pp. 434-437, Aug. 2017.

[5] Y. Li, L. Cai, Y. Li, L. Cai, and Y. Li, "UAV-assisted dynamic coverage in a heterogeneous cellular system," *IEEE Network*, vol. 31, no. 4, pp. 56-61, July 2017.

[6] C. Liu, Z. Chen, J. Tang, J. Xu, and C. Piao, "Energy-efficient UAV control for effective and fair communication coverage: A deep reinforcement learning approach," *IEEE J. Sel. Areas Commun.*, vol. PP, no. 99, pp. 1-11, Aug. 2018.

[7] Y. Zeng, R. Zhang, and J. Teng, "Throughput maximization for UAV-enabled mobile relaying systems," *IEEE Trans. Commun.*, vol. 64. no. 12, pp. 4983-4996, Dec. 2016.

[8] S. Zhang, H. Zhang, Q. He, K. Bian, and L. Song, "Joint trajectory and power optimization for UAV relay networks," *IEEE Commun. Lett.*, vol. 22, no. 1, pp. 161-164, Jan. 2018.

[9] Y. chen, N. Zhao, Z. Ding, and M. Alouini, "Multiple UAVs as relays: multi-hop single link versus multiple dual-hop links," *IEEE J. Sel. Areas Commun.*, vol. PP, no. 99, pp. 1-12, Aug. 2018.

[10] Y. Takahashi, Y. Kawamoto, H. Nishiyama, N. Kato, F. Ono, and R. Miura, "A novel radio resource optimization method for relay-based unmanned aerial vehicles," *IEEE Trans. Wireless Commun.*, vol, PP, no. 99, pp. 1-16, Aug. 2018.

[11] E. Marcosig, J. Giribet, and R. Castro, "Hybrid adaptive control for UAV data collection: A simulation-based design to trade-off resources between stability and communication," in *Proc. of the Winter Simulat. Conf. (WSC)*, pp. 1704-1715, Dec. 2017.

[12] C. Zhan, Y. Zeng, and R. Zhang, "Energy-efficient data collection in UAV enabled wireless sensor network," *IEEE Wirel. Commun. Lett.*, vol. 7, no. 3, pp. 328-331, June 2018.

[13] Y. Cai, F. Cui, Q. Shi, M. Zhao, and G. Li, "Dual-UAV enabled secure communications: Joint trajectory design and user scheduling," *IEEE J. Sel. Areas Commun.*, vol. PP, no. 99, pp. 1-13, Aug. 2018.

[14] M. Cui, G. Zhang, Q. Wu and D. Ng, "Robust trajectory and transmit power design for secure UAV communications," *IEEE Trans. Veh. Technol.*, vol. 67, no. 9, pp. 9042-9046, Sept. 2018.

[15] J. Lee, Y. Su, and C. Shen, "A comparative study of wireless protocols: Bluetooth, UWB, ZigBee, and Wi-Fi," in *Proc. of the IEEE Ind. Electron. Soc. (IECON)*, pp. 46-51, Mar. 2008.

[16] J. Yan, Y. Wan, S. Fu, J. Xie, and S. Li, "RSSI-based decentralized control for robust long-range aerial networking using directional antennaes," *IET Control Theory & Appl.*, vol. 11, no. 11, pp. 1838-1847, July 2017.

[17] J. Chen, J. Xie, Y. Gu, S. Li, and S. Fu, "Long-range and broadband aerial communication using directional antennas (ACDA): design and implementation," *IEEE Trans. Veh. Technol.*, vol. 66, no. 12, pp. 10793-10805, Dec. 2017.

[18] M. Bahat and T. Filik, "GPS-based antenna tracking and signal beamforming system for small UAV platform," in *Proc. of the Signal Proc. and Commun. Appl. Conf. (SIU)*, pp. 1977-1980, Jun. 2015.

[19] J. Zhao, F. Gao, Q. Wu, S. Jin, and Y. We, "Beam tracking for UAV mounted SatCom on-the-move with massive antenna array," *IEEE J. Sel. Areas Commun.*, vol. 36, no. 2, pp. 363-375, Feb. 2018.

[20] T. Tran, M. An, and D. Huynh, "Antenna orientation and range assignment algorithms in directional WSNs," *IEEE/ACM Trans. Networking*, vol. 25, no. 6, pp. 3368-3381, Dec. 2017.

[21] Y. Gu, M. Zhou, S. Fu, and Y. Wan, "Airborne WiFi networks through directional antennae: An experimental study," in *Proc. of IEEE Wirel. Commun. and Networking Conf. (WCNC)*, pp. 1314-1319, Mar. 2015.

[22] J. Xie, F. Aiemrani, Y. Gu, Y. Wan, and S. Fu, "UAV-carried long-distance Wi-Fi communication infrastructure," in *Proc. of AIAA Sci. Technol. Forum and Exposition*, pp. 747-759, Jan. 2016.

[23] Y. Gu, A. Lo, and I. Niemegeers, "A survey of indoor positioning systems for wireless personal networks," *IEEE Commun. Surv. and Tutorials*, vol. 11, no. 1, pp. 13–32, Mar. 2009.

[24] A. Bachrach, S. Prentice, R. He, and N. Roy, "Range-robust autonomous navigation in gps-denied environments," *J. of Field Rob.*, vol. 28. no. 5, pp. 644-666, Aug. 2011.

[25] Y. Lu and S. Velipasalar, "Autonomous footstep counting and traveled distance calculation by mobile devices incorporating camera and accelerometer data," *IEEE Sens. J.*, vol. 17, no. 21, pp. 7157-7166, Sep. 2017.

[26] S. Li, Y. Wan, S. Fu, M. Liu, and H. Wu, "Design and implementation of a remote UAV-based mobile health monitoring system," in *Proc. of the SPIE*, pp. 1-13, Apr. 2017.

[27] B. Min, J. Lewis, E. Matson, and A. Smith, "Heuristic optimization techniques for self-orientation of directional antennas in long-distance point-to-point broadband networks," *Ad Hoc Networks*, vol. 11, no. 8, pp. 2252-2263, 2013.

[28] S. Shahidian and H. Soltanizadeh, "Autonomous trajectory control for limited number of aerial platforms in RF source localization," in *Proc. of the Int. Conf. on Rob. and Mechatron. (ICROM)*, pp. 755-760, Jan. 2016.

[29] B. Min, E. Matson, and J. Jung, "Active antenna tracking system with directional antennas for enhancing wireless communication capabilities of a networked robotic system," *John Wiley and Sons Ltd*, vol. 33, no. 3, pp. 391-406, May 2016.

[30] R. Xu and Ü. Özgüner, "Sliding mode control of a class of underactuated systems," *Automatica*, vol. 44, no. 1, pp. 233–241, Jan. 2008.

[31] S. Shen, Y. Mulgaonkar, N. Michael, and V. Kumar, "Multi-sensor fusion for robust autonomous flight in indoor and outdoor environments with a rotorcraft MAV," in *Proc. of IEEE Int. Conf. on Rob. and Autom.*, pp. 4974-4981, Jun. 2014.

[32] Y. Wan, J. Yan, Z. Lin, V. Sheth, and S. Das, "On the structural perspective of computational effectiveness for quantized consensus in layered UAV networks," *IEEE Trans. on Control of Network Syst.*, vol. PP, no. 99, pp. 1-13, Mar. 2018.

[33] Y. Cui, J. Ren, W. Du, and J. Dai, "UAV target tracking algorithm based on task allocation consensus," *J. Syst. Eng. Electron.*, vol. 27, no. 6, pp. 1207-1218, Dec. 2016.

[34] R. Olfati-Saber and J. Shamma, "Consensus filters for sensor networks and distributed sensor fusion," in *Proc. of IEEE Decis. and Control Conf. (CDC)*, pp. 6698–6703, Jan. 2006.

[35] K. Kolomvatsos, C. Anagnostopoulos, and S. Hadjiefthymiades, "Distributed localized contextual event reasoning under uncertainty," *IEEE Internet of Things J.*, vol. 4, no. 1, pp. 183-191, Feb. 2017.

[36] M. Lippi and M. Mamei, S. Mariani, and F. Zambonelli, "An argumentation-based perspective over the social IoT," *IEEE Internet of Things J.*, vol. 5, no. 4, pp. 2537 - 2547, Aug. 2018.

[37] J. Yan, Z. Xu, X. Luo, C. Chen, and X. Guan, "Feedback-based target localization in underwater sensor networks: A multisensor fusion approach," *IEEE Trans. on Signal and Inf. Proc. over Networks*, vol. PP, no. 99, pp. 1-15, Aug. 2018.

[38] Ubiquiti Networks-NanoStation, 2015. https://www.ubnt.com/airmax/nanostationm/

[39] I. Rao, M. Donga, and M. Chukka, "Design and study of propagation models in wireless communications (GSM) using free space path loss model and hata-okumura model with GUI," *Int. J. of Adv. Res. in Electron. and Commun. Eng.*, vol. 2, no. 12, pp. 1016-1020, Dec. 2013.

[40] C. Zhao and L. Guo, "PID controller design for second order nonlinear uncertain systems," *Sci. China Inf. Sci.*, vol, 60, no. 2, pp. 1-13, Feb. 2017.

[41] C. Luo, S. Mcclean, G. Parr, L. Teacy, and R. Nardi, "UAV position estimation and collision avoidance using the extended kalman filter," *IEEE Trans. Veh. Technol.*, vol. 62, no. 6, pp. 2749-2762, July 2013.

[42] M. Partovibakhsh and G. Liu, "An adaptive unscented Kalman filtering approach for online estimation of model parameters and state-of-charge of Lithium-ion batteries for autonomous mobile robots," *IEEE Trans. Control Syst. Technol.*, vol. 23, no. 1, pp. 357-363, Jan. 2015.

[43] H. Marina, F. Pereda, J. Giron-Sierra, and F. Espinosa, "UAV attitude estimation using unscented kalman filter and TRIAD," *IEEE Trans. Ind. Electron.*, vol. 59, no. 11, pp. 4465-4474, Nov. 2012.

[44] W. Li, G. Wei, F. Han, and Y. Liu, "Weighted average consensus-based unscented kalman filtering," *IEEE Trans. Cybern.*, vol. 46, no. 2, pp. 558-567, Feb. 2016.

[45] K. Xiong, H. Zhang, and C. Chan, "Performance evaluation of UKF-based nonlinear filtering," *Automatica*, vol. 42, no. 2, pp. 261-270, Feb. 2006.

[46] C. Kuo, Automatic Control Systems, 10th ed. McGraw-Hill Education, Feb. 2017.

[47] T. Lefebvre, H. Bruyninckx, and J. Schuller, "Comment on 'A new method for the nonlinear transformation of means and covariances in filters and estimators'[with authors' reply]," *IEEE Trans. Autom. Control*, vol. 47, no. 8, pp. 1406-1409, Aug. 2002.

[48] M. Boutayeb, H. Rafaralahy, and M. Darouach, "Convergence analysis of the extended kalman filter used as an observer for nonlinear deterministic discrete-time systems," *IEEE Trans. Autom. Control*, vol. 42, no. 4, pp. 581-586, Apr. 1997.

[49] M. Rhudy, Y. Gu, and M. Napolitano, "Does the unscented kalman filter converge faster than the extended kalman filter? A counter Example," in *Proc. of AIAA Guidance, Navigation, and Control (GNC)*, pp. 1-8, Aug. 2013.

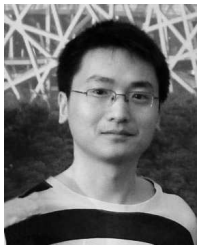

Jing Yan received the B.Eng. degree in Automation from Henan University, Kaifeng, China, in 2008, and the Ph.D. degree in Control Theory and Control Engineering from Yanshan University, Qinhuangdao, China, in 2014. In 2014, he was a Research Assistant with the Key Laboratory of System Control and Information Processing, Ministry of Education, Shanghai Jiaotong University, Shanghai, China. In 2016, he was a research associate with University of Texas at Arlington, Arlington, US. He is currently an Associate Professor with Yanshan University.

His research interests cover in UAV networks, networked teleoperation systems, and cyberphysical systems. He has authored over 20 referred international journal and conference papers. He is the inventor of three patents. He was a recipient of the competitive National Graduate Scholarship from the Ministry of Education of China in 2012. He received the Excellence Paper Award from the National Doctoral Academic Forum of System Control and Information Processing in 2012, the Science and Technology Innovation Award from Yanshan University in 2013, and the Excellence Adviser from Oceanology International Underwater Robot Competition in 2017.

Haiyan Zhao received her B.S. degree in Automation from Yanshan University, Qinhuangdao, China, in 2017. Currently, she is pursuing the Ph.D degree in control theory and control engineering at Yanshan University, Qinhuangdao, China. Her research interests cover in cyberphysical systems, robot control, and networked sensor networks.

Xiaoyuan Luo received the M. Eng. and Ph.D. degrees from the Institute of Electrical Engineering, Yanshan University, Qinhuangdao, China, in 2001 and 2004, respectively. He is currently a professor in Yanshan University. His research interests include fault detection and fault tolerant control, multiagent and networked control systems. He received the Excellence Adviser from Oceanology International Underwater Robot Competition in 2017.

Cailian Chen received the B.Eng. and M.Eng. degrees in Automatic Control from Yanshan University, P. R. China in 2000 and 2002, respectively, and the Ph.D. degree in Control and Systems from City University of Hong Kong, Hong Kong SAR in 2006. She joined Department of Automation, Shanghai Jiao Tong University in 2008 as an Associate Professor. She is now a Full Professor. Prof. Chens research interests include wireless sensor and actuator network and application in industrial automation, vehicular networks and application in intelligent transportation systems, and estimation and control for Multiagent Systems. She has authored and/or coauthored 2 research monographs and over 100 referred international journal and conference papers. She is the inventor of more than 20 patents. Dr. Chen received the IEEE Transactions on Fuzzy Systems Outstanding Paper Award in 2008. She was one of the First Prize Winners of Natural Science Award from The Ministry of Education of China in 2006 and 2016, respectively. She was honored as Changjiang Young Scholar by Ministry of Education of China in 2015 and Excellent Young Researcher by NSF of China in 2016.

Xinping Guan is currently a Chair Professor of Shanghai Jiao Tong University, China, where he is the Deputy Director of University Research Management Office, and the Director of the Key Laboratory of Systems Control and Information Processing, Ministry of Education of China. Before that, he was the Professor and Dean of Electrical Engineering, Yanshan University, China. Prof. Guans current research interests include industrial cyber-physical systems, wireless networking and applications in smart city and smart factory, and underwater sensor networks. He has authored and/or coauthored 4 research monographs, more than 270 papers in IEEE Transactions and other peer-reviewed journals, and numerous conference papers. As a Principal Investigator, he has finished/been working on many national key projects. He is the leader of the prestigious Innovative Research Team of the National Natural Science Foundation of China (NSFC). Dr. Guan is an Executive Committee Member of Chinese Automation Association Council and the Chinese Artificial Intelligence Association Council. He received the First Prize of Natural Science Award from the Ministry of Education of China in 2006 and 2016, respectively, and the Second Prize of the National Natural Science Award of China in 2008. He was a recipient of the IEEE Transactions on Fuzzy Systems Outstanding Paper Award in 2008. He is a National Outstanding Youth honored by NSF of China, Changjiang Scholar by the Ministry of Education of China and State-level Scholar of New Century Bai Qianwan Talent Program of China. Prof. Guan is a Fellow of the Institute of Electrical and Electronics Engineers (IEEE).